Here we demonstrated the involvement of RyRs in the mechanisms underlying mutant htt-induced neuronal death. We found that mutant htt causes Ca^{2+} leak from RyR in transiently transfected HD cellular model and neurons from R6/2 HD model mice. Moreover, expression of RyR stabilizing protein FK506-binding protein 12 (FKBP12) attenuated both Ca^{2+} leak and cell death. Our results provide novel evidence that altered RyR function may contribute to the neurodegeneration in HD.

2. Materials and methods

2.1. Materials

The sources of materials used in this work were as follows: 1,1′-diheptyl-4, 4′-bipyridinium dibromide (DHBP) from TOCRIS Cookson (Bristol, UK), 2-aminoethoxydiphenyl borate (2APB) from Calbiochem Corp. (La Jolla, CA), and thapsigargin from Research Biochemicals Inc. (Natiek, MA). All other materials were obtained either from Wako Pure Chemical Industries, Ltd. (Osaka, Japan) or from Sigma–Aldrich Corp (St. Louis, MO).

2.2. Plasmids

The truncated N-terminal huntingtin (tNhtt) tagged with green fluorescent protein (EGFP) expression constructs pEGFP-tNhtt17Q and pEGFP-tNhtt150Q were provided by N. Nukina [17]. Expression construct pBFP-tNhtt encoding blue fluorescent protein (BFP) was prepared by replacing the EGFP region of pEGFP-tNhtt with the BFP region from pQBI50fC1 vector. The expression plasmids of full-length RyR1 and FLAG-FKBP12 were from G. Meissner [18] and K. Miyazono [19], respectively.

2.3. Cell culture and transfection

Cortical or striatal neurons were prepared from neonatal Sprague–Dawley rats. All the experimental procedures conformed to the guidance set by the committee at the Research Center of Laboratory Animals, Hokkaido University. The tissues were digested with 0.05% trypsin followed by addition of feeding medium (Eagle's minimum essential medium [MEM] supplemented with 5% fetal calf serum [FCS], 5% heat-inactivated horse serum [HS], 10 mM HEPES pH 7.4, 20 mM glucose, 25 U/ml penicillin and 25 μg/ml streptomycin). Mechanically dissociated cells were plated on polyethyleneimine (PEI)-coated plastic plates or glass-cover slips and incubated at 36 °C in a humidified atmosphere of 5% CO_2/95% air. On day 2, Cytosine-β-D-arabinofuranoside (final 2.5 μM) was added to reduce the non-neuronal proliferation, and half of the medium was replaced with fresh serum-free medium at day 4. Cortical or striatal neurons were transfected at day 5–7 as described previously [20]. For co-transfection experiments an equimolar ratio mixture of the plasmids was used. Neuronal expression of tNhtts was confirmed by staining with anti-MAP2 (microtubule-associated protein 2, Sigma) antibody as described previously [6]. Human embryonic kidney 293t cells (293t cells) were cultured in Dulbecco's modified Eagle's medium supplemented with 5% FCS, penicillin and streptomycin.

2.4. Evaluation of cell death

Cortical or striatal neurons were incubated with 5 g/ml ethidium bromide (EtBr) in HEPES-buffered saline (HBS: 140 mM NaCl, 5 mM KCl, 1 mM $CaCl_2$, 1 mM $MgCl_2$, 20 mM HEPES, 1 g/L glucose, pH 7.2) for 5 min. Neurotoxicity is shown as a percentage of the number of neurons stained with EtBr out of that of EGFP-positive neurons. Cell viability of 293t cells was evaluated by dye extrusion with trypan blue as well. Experiments were repeated at least three times and representative results are presented.

2.5. Fluo-3 Ca^{2+} imaging

The cells were loaded with 3 μM fluo-3/AM (Dojindo Laboratories, Kumamoto, Japan) in HBS and 0.04% pluronic F147 (Molecular Probes Inc, Eugene, OR) for 30 min at 36 °C for 293t cells or 27–28 °C for mouse neurons. Ca^{2+} leak through RyR was assessed as described previously with slight modifications [21]. 2APB (final 100 μM) was added to the fluo-3 loading buffer. The glass-cover slips were mounted on a modified Sykes-Moore chamber (Bellco Biotechnology Inc., Vineland, NJ), placed on an inverted microscope (Nikon Diaphoto 300, Nikon). The data was analyzed using the software associated with ARGUS 50 (Hamamatsu Photonics Co., Hamamatsu, Japan). For striatal or cortical neurons from adult mice, HEPES-buffered Hank's balanced salt solution (H-HBSS) was used as a substitute for HBS.

2.6. Preparation of adult dissociated neurons

Striatal or cortical neurons were prepared from 13 to 14 weeks heterozygous transgenic R6/2 male mice (Jackson Laboratories, Bar Harbor, ME) or age-matched controls. Striatum and frontal cerebral cortex were removed from 350 μm coronal brain slices prepared by using McIlwain Tissue Chopper (Mickle Laboratory Engineering Co, Inc, Surrey, UK), and dissociated mechanically in Krebs–Ringer Bicarbonate buffer (KRBB) containing 0.1% bovine serum albumin. The cells were collected and incubated in a feeding medium (50% MEM, 25% H-HBSS, 25% heat-inactivated HS and 25 mM glucose) for 2 days, and then subjected to experiments.

2.7. Statistical analysis

Differences between two groups were analyzed by a two-tailed Student's *t* test. For comparison between more than two groups, ANOVA followed by *post hoc* Turkey's test was used.

3. Results

3.1. Inhibitors of ryanodine receptor protect neurons against toxicity of mutant huntingtin

In this study, we used cortical neurons transiently transfected with wild-type (17Q) or mutant (150Q) truncated N-terminal huntingtin (tNhtt) tagged with enhanced green fluorescent protein (EGFP). EGFP-tNhtt150Q formed intracellular inclusion body in the neurons (Fig. 1A), arrowheads, which is a typical hallmark of HD pathology, and caused neuronal cell death in a polyQ-length-dependent manner (Fig. 1B). By using this model, we explored the role of the inositol 1,4,5-triphosphate receptor (IP3R) and the ryanodine receptor (RyR) in mutant htt-induced neuronal death. We examined the effects of inhibitors of RyR or IP3R and found that dantrolene (Dan), ryanodine (Ry), 1,1′-diheptyl-4,4′-bipyridinium dibromide (DHBP) and ruthenium red (RR), all inhibitors of RyRs, significantly suppress mutant htt-induced neuronal death (Fig. 1C). In contrast, 2-aminoethoxydiphenyl borate (2APB), an inhibitor of IP3Rs, failed to protect these neurons. The protective effect of Dan was abolished by 4-chloro-m-cresol (CMC), a potent activator of RyRs, confirming that the effect of Dan is indeed mediated by inhibition of RyR (Fig. 1D). It was also found that Dan effectively attenuated mutant htt-induced cell death of striatal neurons (Fig. 1E). These results indicate that inhibition of Ca^{2+} release from RyRs, but not IP3Rs, attenuates neuronal death induced by mutant htt.

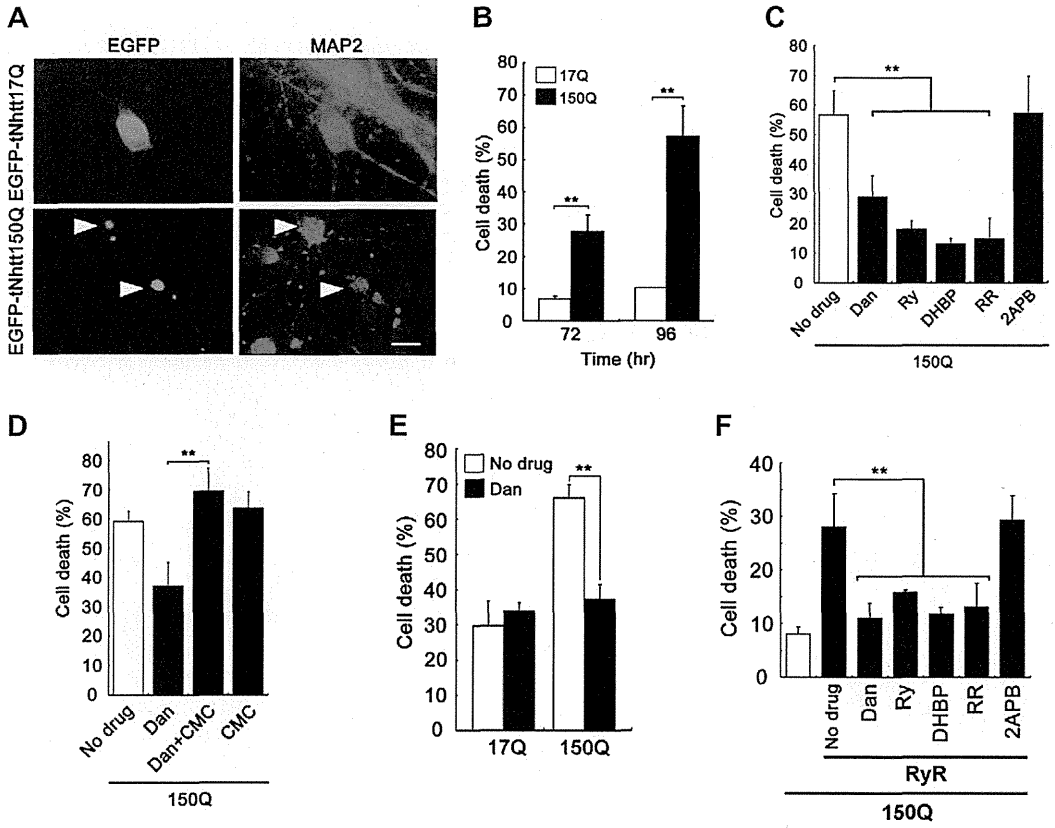

Fig. 1. Blockade of ryanodine receptor (RyR) attenuates neuronal cell death induced by mutant huntingtin (htt). (A) Immunofluorescence analysis. Cortical neurons transfected with EGFP-tagged truncated N-terminal huntingtin 17Q (EGFP-tNhtt17Q) and 150Q (EGFP-tNhtt150Q) were stained with the neuronal marker MAP2. Arrowheads indicate mutant htt inclusions. Bar, 10 μm. (B) Time- and length-dependency of mutant htt-induced neuronal death. (C) Suppression of mutant htt-induced neuronal death by inhibition of RyRs. Cortical neurons transfected with EGFP-tNhtt150Q (150Q) were treated with RyR inhibitors such as dantrolene (Dan, 30 μM), ryanodine (Ry, 10 μM), 1,1′-diheptyl-4,4′-bipyridinium dibromide (DHBP, 50 nM) or ruthenium red (RR, 10 nM). Inositol 1,4,5-triphosphate receptors (IP3Rs) inhibitor 2-aminoethoxydiphenyl borate (2APB, 10 μM) did not show any effects. (D) Counteracting effect of RyR activator 4-chloro-m-cresol (CMC) on the protective effect of Dan. Cortical neurons were treated with Dan (30 μM), CMC (10 μM), or both. (E) Protective effect of Dan in striatal neurons. Concentration of Dan was 30 μM. (F) Potentiation of mutant htt toxicity by expression of RyR1. HEK 293t cells bearing no endogenous RyR, were co-transfected with EGFP-tNhtt150Q (150Q) and RyR1. Concentration of the drugs was same as C. The mean ± SD ($n = 3$). $^{**}p < 0.01$.

To obtain direct evidence that RyRs actually mediate the toxicity of mutant htt, we next investigated the effect of RyR expression on mutant htt toxicity. Co-expression of EGFP-tNhtt150Q and RyR1, which has target site for Dan inhibition [22], and is reported to increase in the caudate nucleus of HD patients [23], significantly increased cell death of HEK 293t (293t) cells bearing no endogenous RyRs. We further confirmed that this increase was suppressed by RyRs inhibitors, but not with IP3Rs inhibitor (Fig. 1F). Taken together, we concluded that abnormal Ca^{2+} release through RyR1 is induced by mutant htt and involved in mutant htt-induced neuronal cell death.

3.2. Mutant htt causes abnormal Ca^{2+} leak through RyRs

We moved on to measure the level of cytoplasmic calcium ($[Ca^{2+}]_i$) upon activation of RyRs to examine if there is any dysfunction regarding Ca^{2+} release from RyR expressing mutant htt. The cells co-expressing blue fluorescent protein (BFP)-tNhtts and RyR1 responded to caffeine, which activates RyRs to release Ca^{2+} from ER to cytoplasm, by rapid increases in $[Ca^{2+}]_i$ 24 h after transfection, and the responses were similar between wild-type (Q17) and mutant (Q150) htt (Fig. 2A and B). However, the cells expressing mutant htt became to poorly respond to this stimulation at 48 h, and these cells failed to respond by 72 h.

These results raise the possibility that the internal Ca^{2+} store might be depleted under these conditions by enhanced spontaneous Ca^{2+} release (Ca^{2+} leak). Ca^{2+} levels of cytoplasm and ER is balanced by uptake through SERCAs (sarco/endoplasmic reticulum Ca^{2+} pumps) and release through RyRs and IP3Rs (Fig. 3A). Therefore, Ca^{2+} leak through RyR could be evaluated by measuring $[Ca^{2+}]_i$ increase under treatment with thapsigargin (TG), an inhibitor of SERCAs, following pretreatment with 2APB, an inhibitor of IP3Rs [21]. Upon these treatments, there was a slight increase in $[Ca^{2+}]_i$ in the cells expressing wild-type htt and RyR1 (17Q), which indicates spontaneous Ca^{2+} release through RyR1. Compared with this, there was a large increase in $[Ca^{2+}]_i$ in the cells expressing mutant htt and RyR1 (150Q, Fig. 3B and C). This $[Ca^{2+}]_i$ increase was suppressed by treatment with RyR inhibitor DHBP (150Q+DHBP), suggesting that excessive Ca^{2+} leak through RyR is induced by mutant htt.

Next we further sought to obtain evidence that abnormal Ca^{2+} leak from RyRs occurs in a well-established animal model as well. Striatal or cortical neurons were prepared from 13- to 14-weeks-old R6/2 HD model mice expressing exon1 of htt with 144 repeats of polyQ tract, and subjected to Ca^{2+} imaging. The neurons from R6/2 (R6/2) mice, but not those from age-matched wild-type mice (WT), showed a gradual increase in $[Ca^{2+}]_i$ levels following application of TG (Fig. 3D) and there was a significant difference in relative

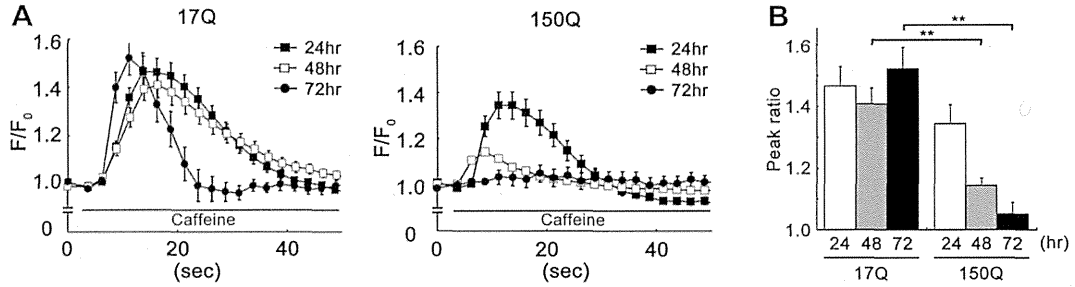

Fig. 2. Caffeine-sensitive Ca^{2+} store declines in the cells expressing mutant htt. (A) Cytoplasmic Ca^{2+} increase upon treatment with an activator of the RyR. HEK 293t cells were co-transfected with RyR1 and blue fluorescent protein (BFP)-tagged tNhtt17Q (17Q) or 150Q (150Q) for 24, 48 or 72 h, and then loaded with calcium indicator fluo-3. Fluo-3 fluorescence of BFP-positive cells was monitored following treatment with caffeine (25 mM). (B) Peak values of caffeine responses in A. A maximal value for F/F_0 was calculated for caffeine responses of each cell. The mean ± SE (n = 16–26 cells). $^{**}p < 0.01$.

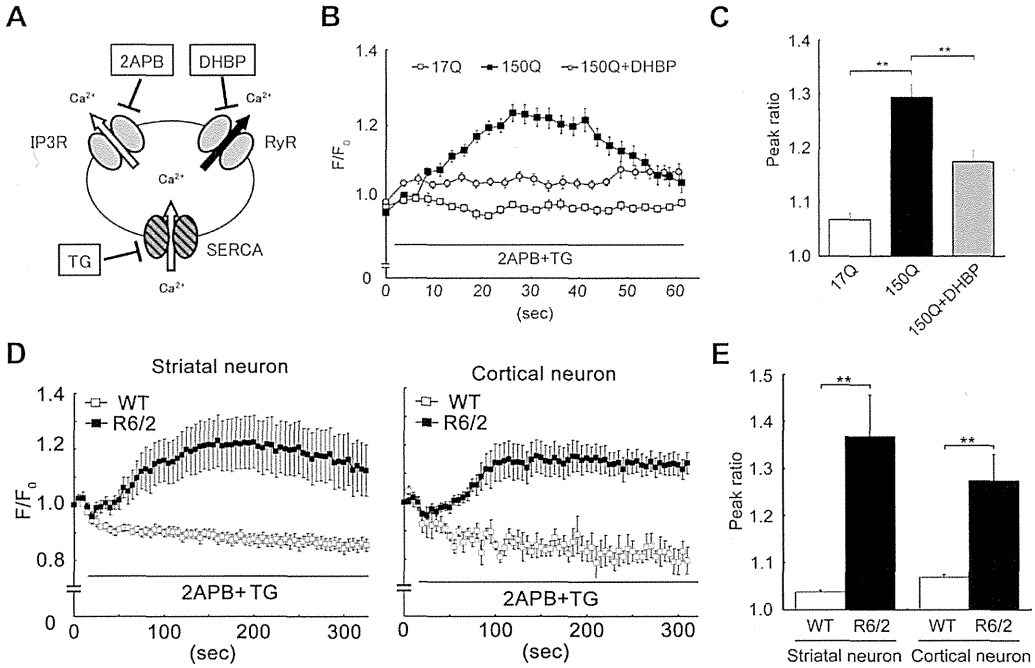

Fig. 3. Mutant htt induces abnormal Ca^{2+} leak through RyRs. (A) Schematic drawing of Ca^{2+} flow between cytoplasm and ER. Ca^{2+} leak through RyR was assessed by measurement of cytoplasmic Ca^{2+} increase upon treatment with thapsigargin (TG), an inhibitor of SERCAs (ER Ca^{2+} pumps), and 2APB, an inhibitor of IP3Rs. (B) Abnormal Ca^{2+} leak through RyR in the cells expressing mutant htt. HEK 293t cells were transfected with RyR1 and BFP-tNhtt17Q (17Q) or 150Q (150Q). At 24 h of transfection, the cells were loaded with fluo-3 in the presence of 100 μM 2APB and then cytoplasmic Ca^{2+} levels were measured following treatment with 1 μM TG. Enhanced Ca^{2+} increase of mutant htt-expressing cells was suppressed by RyR inhibitor DHBP (50 nM). The mean ± SE (n = 13–29). (C) Maximal value of F/F_0 in B. (D) Abnormal Ca^{2+} leak in striatal or cortical neurons from R6/2 HD model mice. The neurons prepared from 13- to 14-week-old wild-type (WT, n = 15) or R6/2 mice (R6/2, n = 14) were incubated with 3 μM fluo-3 and 100 μM 2APB. Then, cytoplasmic Ca^{2+} levels were measured following treatment with 0.5 μM TG. (E) Quantification of the results in D. The mean ± SE. $^{**}p < 0.01$.

peak ratios of these responses between R6/2 and wild-type mice (Fig. 3E). Taken together, these results show that mutant htt induces enhanced Ca^{2+} leak through RyRs in the HD pathogenesis.

3.3. Expression of RyR stabilizer FKBP12 suppresses mutant htt-induced abnormal Ca^{2+} leak and cell death

We further examined whether stabilization of RyR1 could suppress abnormal Ca^{2+} leak and mutant htt-induced cell death. It is well-known that FK506-binding protein 12 (FKBP12), a member of immunophilin family, physically interacts and stabilizes RyR1 by decreasing channel open probability, playing the role for endogenous RyR stabilizer [24]. Therefore, we co-expressed FKBP12 with mutant htt, and found that mutant htt-induced Ca^{2+} leak through RyR1 was effectively suppressed by FKBP12 in 293t cells (Fig. 4A and B). Consistent with these results, FKBP12 decreased cell death of 293t cells, primary cultured cortical and striatal neurons (Fig. 4C and D), suggesting that stabilization of RyR channel function protects neurons against mutant htt toxicity.

4. Discussion

Here we have shown that inhibitors of RyRs attenuate cell death induced by mutant htt. Mutant htt caused Ca^{2+} leak from RyR1 followed by depletion of Ca^{2+} store in the ER, and expression of RyR stabilizer FKBP12 suppressed both Ca^{2+} leak and cell death. From these results we concluded that abnormal Ca^{2+} leak from RyRs may contribute to neuronal death in HD.

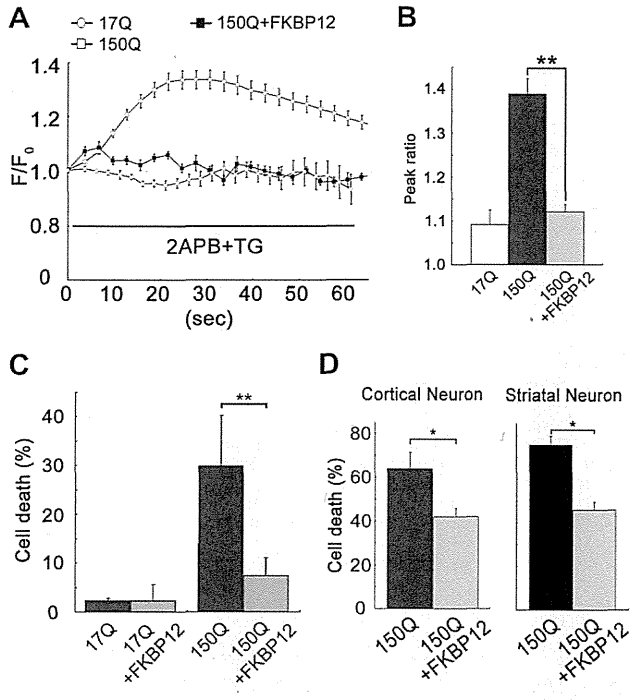

Fig. 4. Expression of RyR stabilizer FK506-binding protein 12 (FKBP12) suppresses mutant htt-induced abnormal Ca^{2+} leak and cell death. (A) Suppression of abnormal Ca^{2+} leak from RyR by FKBP12. HEK293t cells were co-transfected with RyR1 and BFP-tNhtt17Q (17Q), RyR1 and BFP-tNhtt150Q (150Q), or RyR1, BFP-tNhtt150Q and FKBP12 (150Q+FKBP12). Ca^{2+} leak was assessed at 48 h of transfection. The mean ± SE (n = 19–21). (B) Quantification of the results shown in A. (C) Suppression of mutant htt-induced cell death by FKBP12 in HEK 293t cells. Cell viability was evaluated 96 h after transfection. The mean ± SD (n = 3). (D) Attenuation of mutant htt-induced neuronal death by expression of FKBP12. Primary cultured cortical or striatal neurons were transfected for 96 h and cell viability was evaluated. The mean ± SD (n = 3). $^*p < 0.05$,$^{**}p < 0.01$.

To our knowledge, this study is the first report suggesting that Ca^{2+} leak through RyR contributes to pathogenesis of HD. Ca^{2+} leak from RyR1 has mainly been reported in muscular diseases such as malignant hyperthermia and muscular dystrophies. In these conditions, PKA (cAMP-dependent protein kinase)-dependent phosphorylation, oxidation or nitrosylation of RyR is shown to cause dissociation of FKBP proteins from the channels resulting in Ca^{2+} leak [25]. Although we have not assessed the status of RyR, there are several reports implicating that similar modification of RyR might be induced by mutant htt. For instance, increased activity of PKA [26] and nitric oxide synthase was found in R6/1 HD model mice [27] and increased reactive oxygen species and nitric oxide production was shown in a htt-expressing cellular model [28]. It has also been reported that FKBP12 mRNA level was decreased, whereas the expression of RyR1 increased, in caudate nucleus of grade 1 HD patient [23].

Then, how does Ca^{2+} leak induce neuronal cell death? Continuous Ca^{2+} leak might cause elevated cytosolic Ca^{2+} levels, which is observed in a YAC mouse model and R6/2 mouse [29,30]. Elevated cytosolic Ca^{2+} might lead mitochondrial depolarization through Ca^{2+} overload that cause energy disruption. Ca^{2+} overload also induces the release of cytochrome c that leads subsequent apoptotic pathways. It is reported that mitochondria of mutant htt-expressing cells show increased Ca^{2+} sensitivity of the permeability transition pore [12]. Not only mitochondrial damage, but also Ca^{2+} leak might amplify the toxicity of mutant htt in other ways. For example, elevated cytosolic Ca^{2+} may cause Calpain activation leading to generate toxic fragments [31]. Moreover, if the reduction in ER Ca^{2+} levels occurs, ER stress may be induced and eventually lead to cell death [32].

In addition to Ca^{2+} leak, we also found that caffeine-sensitive Ca^{2+} store might be depleted in mutant htt-expressing cells. Because Ca^{2+} leak was observed prior to declined caffeine responses in our cellular model (Figs. 3 and 4), continuous Ca^{2+} leak might result in Ca^{2+} depletion of caffeine-sensitive stores. Since RyR is considered to play a pivotal role in neuronal functions including excitation, neurotransmitter release, synaptic plasticity [33], stabilization of RyR might be effective not only in neuronal death but also in neuronal dysfunction of HD.

Currently there is no treatment for attenuating or reversing HD. Our results strongly indicate that dantrolene or other similar RyR inhibitors may be beneficial for HD patients. Notably, dantrolene is one of the clinically approved drugs and its neuroprotective effect has been shown in other neurological disease models including spinocerebellar ataxia type 2 and type 3, Alzheimer's disease and ischemia [9,10,14,15]. This study revealed novel mechanism of action whereby dantrolene attenuate neurodegeneration through suppression of Ca^{2+} leak from RyR and further support the notion that dantrolene should be potential therapeutic agent for the treatment of HD.

Acknowledgments

We would like to thank Dr. Nukina, Dr. Meissner and Dr. Miyazono for providing expression vectors. This work was supported by Hokkaido University Clark Memorial Foundation (MS), Core Research for Evolutional Science and Technology (CREST) of Japan Science and Technology Agency (YN) and a fund from the Japanese Ministry of Education, Culture, Sports, Science and Technology (TK). MS is an awardee of the fellowship by the COE program for Advance Life Science on the base of Bioscience and Nanotechnology Hokkaido University.

References

[1] P.O. Bauer, N. Nukina, The pathogenic mechanisms of polyglutamine diseases and current therapeutic strategies, J. Neurochem. 110 (2009) 1737–1765.
[2] J.P. Vonsattel, R.H. Myers, T.J. Stevens, R.J. Ferrante, E.D. Bird, E.P. Richardson Jr., Neuropathological classification of Huntington's disease, J. Neuropathol. Exp. Neurol. 44 (1985) 559–577.
[3] A. Lunkes, K.S. Lindenberg, L. Ben-Haiem, C. Weber, D. Devys, G.B. Landwehrmeyer, J.L. Mandel, Y. Trottier, Proteases acting on mutant huntingtin generate cleaved products that differentially build up cytoplasmic and nuclear inclusions, Mol. Cells 10 (2002) 259–269.
[4] Y. Nagai, H.A. Popiel, Conformational changes and aggregation of expanded polyglutamine proteins as therapeutic targets of the polyglutamine diseases: exposed beta-sheet hypothesis, Curr. Pharm. Des. 14 (2008) 3267–3279.
[5] I. Bezprozvanny, M.R. Hayden, Deranged neuronal calcium signaling and Huntington disease, Biochem. Biophys. Res. Commun. 322 (2004) 1310–1317.
[6] M. Suzuki, T. Koike, Early apoptotic and late necrotic components associated with altered Ca^{2+} homeostasis in a peptide-delivery model of polyglutamine-induced neuronal death, J. Neurosci. Res. 80 (2005) 549–561.
[7] M.P. Mattson, F.M. LaFerla, S.L. Chan, M.A. Leissring, P.N. Shepel, J.D. Geiger, Calcium signaling in the ER: its role in neuronal plasticity and neurodegenerative disorders, Trends Neurosci. 23 (2000) 222–229.
[8] T.S. Tang, H. Tu, E.Y. Chan, A. Maximov, Z. Wang, C.L. Wellington, M.R. Hayden, I. Bezprozvanny, Huntingtin and huntingtin-associated protein 1 influence neuronal calcium signaling mediated by inositol-(1,4,5) triphosphate receptor type 1, Neuron 39 (2003) 227–239.
[9] X. Chen, T.S. Tang, H. Tu, O. Nelson, M. Pook, R. Hammer, N. Nukina, I. Bezprozvanny, Deranged calcium signaling and neurodegeneration in spinocerebellar ataxia type 3, J. Neurosci. 28 (2008) 12713–12724.
[10] J. Liu, T.S. Tang, H. Tu, O. Nelson, E. Herndon, D.P. Huynh, S.M. Pulst, I. Bezprozvanny, Deranged calcium signaling and neurodegeneration in spinocerebellar ataxia type 2, J. Neurosci. 29 (2009) 9148–9162.
[11] X. Chen, J. Wu, S. Lvovskaya, E. Herndon, C. Supnet, I. Bezprozvanny, Dantrolene is neuroprotective in Huntington's disease transgenic mouse model, Mol. Neurodegener. 6 (2011) 81.
[12] D. Lim, L. Fedrizzi, M. Tartari, C. Zuccato, E. Cattaneo, M. Brini, E. Carafoli, Calcium homeostasis and mitochondrial dysfunction in striatal neurons of Huntington disease, J. Biol. Chem. 283 (2008) 5780–5789.

[13] P.O. Bauer, R. Hudec, S. Ozaki, M. Okuno, E. Ebisui, K. Mikoshiba, N. Nukina, Genetic ablation and chemical inhibition of IP3R1 reduce mutant huntingtin aggregation, Biochem. Biophys. Res. Commun. 416 (2011) 13–17.
[14] B. Oules, D. Del Prete, B. Greco, X. Zhang, I. Lauritzen, J. Sevalle, S. Moreno, P. Paterlini-Brechot, M. Trebak, F. Checler, F. Benfenati, M. Chami, Ryanodine receptor blockade reduces amyloid-beta load and memory impairments in Tg2576 mouse model of Alzheimer disease, J. Neurosci. 32 (2012) 11820–11834.
[15] F. Li, T. Hayashi, G. Jin, K. Deguchi, S. Nagotani, I. Nagano, M. Shoji, P.H. Chan, K. Abe, The protective effect of dantrolene on ischemic neuronal cell death is associated with reduced expression of endoplasmic reticulum stress markers, Brain Res. 1048 (2005) 59–68.
[16] S. Muehlschlegel, J.R. Sims, Dantrolene: mechanisms of neuroprotection and possible clinical applications in the neurointensive care unit, Neurocrit. Care 10 (2009) 103–115.
[17] G.H. Wang, K. Mitsui, S. Kotliarova, A. Yamashita, Y. Nagao, S. Tokuhiro, T. Iwatsubo, I. Kanazawa, N. Nukina, Caspase activation during apoptotic cell death induced by expanded polyglutamine in N2a cells, Neuroreport 10 (1999) 2435–2438.
[18] L. Gao, A. Tripathy, X. Lu, G. Meissner, Evidence for a role of C-terminal amino acid residues in skeletal muscle Ca^{2+} release channel (ryanodine receptor) function, FEBS Lett. 412 (1997) 223–226.
[19] T. Okadome, E. Oeda, M. Saitoh, H. Ichijo, H.L. Moses, K. Miyazono, M. Kawabata, Characterization of the interaction of FKBP12 with the transforming growth factor-beta type I receptor in vivo, J. Biol. Chem. 271 (1996) 21687–21690.
[20] M. Jiang, L. Deng, G. Chen, High Ca(2+)-phosphate transfection efficiency enables single neuron gene analysis, Gene Ther. 11 (2004) 1303–1311.
[21] X. Liu, M.J. Betzenhauser, S. Reiken, A.C. Meli, W. Xie, B.X. Chen, O. Arancio, A.R. Marks, Role of leaky neuronal ryanodine receptors in stress- induced cognitive dysfunction, Cell 150 (2012) 1055–1067.
[22] F. Zhao, P. Li, S.R. Chen, C.F. Louis, B.R. Fruen, Dantrolene inhibition of ryanodine receptor Ca^{2+} release channels molecular mechanism and isoform selectivity, J. Biol. Chem. 276 (2001) 13810–13816.
[23] A. Hodges, A.D. Strand, A.K. Aragaki, A. Kuhn, T. Sengstag, G. Hughes, L.A. Elliston, C. Hartog, D.R. Goldstein, D. Thu, Z.R. Hollingsworth, F. Collin, B. Synek, P.A. Holmans, A.B. Young, N.S. Wexler, M. Delorenzi, C. Kooperberg, S.J. Augood, R.L. Faull, J.M. Olson, L. Jones, R. Luthi-Carter, Regional and cellular gene expression changes in human Huntington's disease brain, Hum. Mol. Genet. 15 (2006) 965–977.
[24] A.B. Brillantes, K. Ondrias, A. Scott, E. Kobrinsky, E. Ondriasova, M.C. Moschella, T. Jayaraman, M. Landers, B.E. Ehrlich, A.R. Marks, Stabilization of calcium release channel (ryanodine receptor) function by FK506-binding protein, Cell 77 (1994) 513–523.
[25] S.E. Lehnart, Novel targets for treating heart and muscle disease: stabilizing ryanodine receptors and preventing intracellular calcium leak, Curr. Opin. Pharmacol. 7 (2007) 225–232.
[26] A. Giralt, A. Saavedra, O. Carreton, X. Xifro, J. Alberch, E. Perez-Navarro, Increased PKA signaling disrupts recognition memory and spatial memory: role in Huntington's disease, Hum. Mol. Genet. 20 (2011) 4232–4247.
[27] F. Perez-Severiano, B. Escalante, P. Vergara, C. Rios, J. Segovia, Age-dependent changes in nitric oxide synthase activity and protein expression in striata of mice transgenic for the Huntington's disease mutation, Brain Res. 951 (2002) 36–42.
[28] W.J. Firdaus, A. Wyttenbach, P. Giuliano, C. Kretz-Remy, R.W. Currie, A.P. Arrigo, Huntingtin inclusion bodies are iron-dependent centers of oxidative events, FEBS J. 273 (2006) 5428–5441.
[29] J.G. Hodgson, N. Agopyan, C.A. Gutekunst, B.R. Leavitt, F. LePiane, R. Singaraja, D.J. Smith, N. Bissada, K. McCutcheon, J. Nasir, L. Jamot, X.J. Li, M.E. Stevens, E. Rosemond, J.C. Roder, A.G. Phillips, E.M. Rubin, S.M. Hersch, M.R. Hayden, A YAC mouse model for Huntington's disease with full-length mutant huntingtin, cytoplasmic toxicity, and selective striatal neurodegeneration, Neuron 23 (1999) 181–192.
[30] O. Hansson, E. Guatteo, N.B. Mercuri, G. Bernardi, X.J. Li, R.F. Castilho, P. Brundin, Resistance to NMDA toxicity correlates with appearance of nuclear inclusions, behavioural deficits and changes in calcium homeostasis in mice transgenic for exon 1 of the Huntington gene, Eur. J. Neurosci. 14 (2001) 1492–1504.
[31] J. Gafni, L.M. Ellerby, Calpain activation in Huntington's disease, J. Neurosci. 22 (2002) 4842–4849.
[32] H.N. Nguyen, C. Wang, D.C. Perry, Depletion of intracellular calcium stores is toxic to SH-SY5Y neuronal cells, Brain Res. 924 (2002) 159–166.
[33] S. Bardo, M.G. Cavazzini, N. Emptage, The role of the endoplasmic reticulum Ca^{2+} store in the plasticity of central neurons, Trends Pharmacol. Sci. 27 (2006) 78–84.

OPEN ACCESS Freely available online

PLoS one

Knockdown of the *Drosophila* Fused in Sarcoma (FUS) Homologue Causes Deficient Locomotive Behavior and Shortening of Motoneuron Terminal Branches

Hiroshi Sasayama[1☯], Mai Shimamura[2,3☯], Takahiko Tokuda[1,4*], Yumiko Azuma[1], Tomokatsu Yoshida[1], Toshiki Mizuno[1], Masanori Nakagawa[1], Nobuhiro Fujikake[5], Yoshitaka Nagai[5], Masamitsu Yamaguchi[2,3*]

1 Department of Neurology, Graduate School of Medical Science, Kyoto Prefectural University of Medicine, Kamigyo-ku, Kyoto, Japan, **2** Department of Applied Biology, Kyoto Institute of Technology, Matsugasaki, Sakyo-ku, Kyoto, Japan, **3** Insect Biomedical Research Center, Kyoto Institute of Technology, Matsugasaki, Sakyo-ku, Kyoto, Japan, **4** Department of Molecular Pathobiology of Brain Diseases, Graduate School of Medical Science, Kyoto Prefectural University of Medicine, Kamigyo-ku, Kyoto, Japan, **5** Department of Degenerative Neurological Diseases, National Institute of Neuroscience, National Center of Neurology and Psychiatry, Kodaira, Tokyo, Japan

Abstract

Mutations in the fused in sarcoma/translated in liposarcoma gene (FUS/TLS, FUS) have been identified in sporadic and familial forms of amyotrophic lateral sclerosis (ALS). FUS is an RNA-binding protein that is normally localized in the nucleus, but is mislocalized to the cytoplasm in ALS, and comprises cytoplasmic inclusions in ALS-affected areas. However, it is still unknown whether the neurodegeneration that occurs in ALS is caused by the loss of FUS nuclear function, or by the gain of toxic function due to cytoplasmic FUS aggregation. Cabeza (Caz) is a *Drosophila* orthologue of human FUS. Here, we generated *Drosophila* models with *Caz* knockdown, and investigated their phenotypes. In wild-type *Drosophila*, Caz was strongly expressed in the central nervous system of larvae and adults. Caz did not colocalize with a presynaptic marker, suggesting that Caz physiologically functions in neuronal cell bodies and/or their axons. Fly models with neuron-specific *Caz* knockdown exhibited reduced climbing ability in adulthood and anatomical defects in presynaptic terminals of motoneurons in third instar larvae. Our results demonstrated that decreased expression of *Drosophila* Caz is sufficient to cause degeneration of motoneurons and locomotive disability in the absence of abnormal cytoplasmic Caz aggregates, suggesting that the pathogenic mechanism underlying FUS-related ALS should be ascribed more to the loss of physiological FUS functions in the nucleus than to the toxicity of cytoplasmic FUS aggregates. Since the *Caz*-knockdown *Drosophila* model we presented recapitulates key features of human ALS, it would be a suitable animal model for the screening of genes and chemicals that might modify the pathogenic processes that lead to the degeneration of motoneurons in ALS.

Citation: Sasayama H, Shimamura M, Tokuda T, Azuma Y, Yoshida T, et al. (2012) Knockdown of the *Drosophila* Fused in Sarcoma (FUS) Homologue Causes Deficient Locomotive Behavior and Shortening of Motoneuron Terminal Branches. PLoS ONE 7(6): e39483. doi:10.1371/journal.pone.0039483

Editor: Koichi M. Iijima, Thomas Jefferson University, United States of America

Received January 9, 2012; **Accepted** May 21, 2012; **Published** June 19, 2012

Funding: TT is supported by Grants-in-Aid from the Research Committee of CNS Degenerative Diseases, the Ministry of Health, Labour and Welfare of Japan. The funders had no role in study design, data collection and analysis, decision to publish, or preparation of the manuscript.

Competing Interests: The authors have declared that no competing interests exist.

* E-mail: ttokuda@koto.kpu-m.ac.jp (TT); myamaguc@kit.ac.jp (MY)

☯ These authors contributed equally to this work.

Introduction

Amyotrophic lateral sclerosis (ALS) is a devastating neurodegenerative disease that is characterized by degeneration of motor neurons, which leads to progressive muscle weakness and eventually fatal paralysis, typically within 1 to 5 years after disease onset [1]. Frontotemporal lobar degeneration (FTLD) is a clinically diverse dementia syndrome, with phenotypes that include behavioral changes, semantic dementia and progressive non-fluent aphasia [2]. Although these two diseases are clinically distinct and affect different parts of the central nervous system, it has been long thought that these two diseases are related since ALS patients often develop cognitive deficits with frontotemporal features and FTLD patients can present symptoms of motor neuron disease [3,4]. This hypothesis, which was derived from clinical observations, has been biochemically confirmed by identification of the 43 kDa TAR-DNA-binding protein (TDP-43) as the major aggregating protein in subtypes of both ALS and FTLD (ALS-TDP and FTLD-TDP, respectively) [5,6]. Moreover, over 30 different mutations in the TDP-43 gene (*TARDBP*) have been identified in various sporadic and familial ALS patients [7–12], and subsequently TDP-43 mutations were reported in various FTLD-TDP cases [13,14]. Shortly after the identification of mutations in TDP-43 in ALS cases, mutations in another gene encoding an RNA-binding protein, FUS (fused in sarcoma; also known as TLS, translocated in liposarcoma), were identified in cases with familial ALS (ALS-FUS) [15,16]. Both dominantly and recessively inherited *FUS* mutations have been reported in familial ALS [15], and *FUS* mutations may be more common than *TARDBP* mutations in familial ALS [17]. Additional mutations in *FUS* have recently been identified in sporadic ALS cases and in a subset of FTLD cases (FTLD-FUS) [18,19]. FUS is normally a nuclear protein, but cytoplasmic FUS-immunoreactive inclusions were demonstrated in lower motor neurons of ALS patients

harboring *FUS* mutations [16]. Cytoplasmic aggregation of wild-type FUS was subsequently reported as the prominent disease phenotype in other neurodegenerative diseases such as basophilic inclusion body disease [20], some types of juvenile ALS [21], and in the majority of tau- and TDP43-negative FTLD [22]. The identification of these two RNA-binding proteins that aggregate and are sometimes mutated in ALS and FTLD gave rise to the emerging concept that disturbances in RNA regulation may play a major role in the pathogenesis of ALS and FTLD [23]. Moreover, FUS aggregation is also demonstrated in Huntington's disease, spinocerebellar ataxia types 1, 2, and 3, and dentatorubropallidoluysian atrophy [24,25]. These findings suggest an important role for FUS aggregation in the pathogenesis of neurodegenerative diseases beyond ALS and FTLD.

FUS is a ubiquitously expressed, 526 amino acid protein that was initially identified as a proto-oncogene, and which causes liposarcoma due to chromosomal translocation [26]. FUS is an RNA-binding protein that is implicated in multiple aspects of RNA metabolism including microRNA processing, RNA splicing, trafficking and translation [23,27,28]. FUS shows nuclear and cytoplasmic expression and shuttles between the nucleus and the cytoplasm [27,29]. In neurons, FUS is localized to the nucleus but it is transported to dendritic spines at excitatory post-synapses in a complex with RNA and other RNA-binding proteins [30]. Similar to TDP-43, FUS comprises a glycine-rich domain (GRD), an RNA-recognition-motif (RRM) domain and a nuclear localization sequence (NLS). ALS/FTLD-associated mutations cluster in the C-terminal region of the FUS protein that contains a non-classical R/H/KX$_{2-5}$PY NLS motif [31] as well as in the GRD motif that is important for protein-protein interactions and also exists in the C-terminal region of TDP-43. Most pathogenic mutations of the *TARDBP* gene cluster in this GRD motif. The only known genetic cause for ALS/FTLD with FUS pathology is mutations in the *FUS* gene itself. The *FUS* mutations in the NLS-containing C-terminal region lead to redistribution of the FUS protein from the nucleus to the cytoplasm [32–35]. These findings suggest that the loss of physiological nuclear functions of FUS that involve RNA regulation may contribute to the pathogenesis of ALS/FTLD.

There is a single homolog for each of human FUS and TDP-43 in *Drosophila*, named Cabeza (Caz) and TBPH, respectively. The *Caz* gene is located on the X chromosome, and is a member of an RNA binding proteins that are conserved from fly to man. *In situ* hybridization and immunohistochemical analyses demonstrated that Caz mRNA and protein are enriched in the brain and CNS during embryogenesis, and the Caz protein was detected in the nuclei of several larval tissues and in imaginal discs [36]. The full-length recombinant Caz protein and its RRM domain are capable of binding RNA in vitro [36]. These findings suggest that Caz is a nuclear RNA binding protein that may play an important role in the regulation of RNA metabolism during fly development. Feiguin et al. reported that *Drosophila* lacking TBPH presented deficient locomotive behaviors, reduced life span and anatomical defects at neuromuscular junctions (NMJ), suggesting that a loss of TDP-43 nuclear functions could be a causative factor of the neurodegeneration observed in patients with ALS/FTLD [37].

As mentioned above, the loss of the nuclear function of FUS or TDP-43 plays an important role in the pathogenesis of ALS/FTLD. However, aggregation of TDP-43 or FUS may by itself be toxic due to a toxic gain-of-function associated with the formation of cytoplasmic aggregates of those proteins, which would trap vital proteins and/or RNAs and might disturb cellular homeostasis. Thus, it remains unclear whether it is the loss of FUS nuclear function or the gain of toxic function resulting from FUS aggregation that is the mechanism that underlies the primary abnormality that leads to the neurodegeneration that occurs in ALS/FTLD. The existence of both dominantly and recessively inherited *FUS* mutations in familial ALS has provoked further controversy regarding whether the underlying pathogenic mechanism of ALS/FTLD is due to gain-of-toxic-function or loss-of-nuclear function [15,19,38]. Here, we investigated phenotypes of fly models with knockdown of the *Drosophila* FUS homologue, *Caz* gene, to provide supporting evidence for our hypothesis that the pathogenesis of ALS/FTLD may be due more to the loss of physiological FUS functions than to the toxicity of its cytoplasmic aggregates. Neuron-specific knockdown of the *Drosophila Caz* gene reduced the climbing abilities of adult flies as well as caused anatomical defects, such as a reduced length of synaptic branches, in presynaptic terminals of motoneurons in third instar larvae, suggesting that decreased expression of the *Drosophila* FUS homologue may be sufficient for development of the degeneration of motoneurons and for the deficient locomotive behavior in this model fly.

Results

Comparison of the amino acid sequence of human FUS and *Drosophila* Caz

The amino acid sequence of *Drosophila* Caz was retrieved from the Flybase and was compared with that of human FUS using BLAST and FASTA (Figure 1). The identity and the similarity of the amino acid sequences of Caz and FUS are 44.9% and 62.3%, respectively. Regarding conservation of specific FUS domains, the RRM domain, which is known to bind RNAs, as well as the zinc finger domain, are both highly conserved between human FUS and *Drosophila* Caz, showing 50% and 63% identity, respectively. The similarity of the human and *Drosophila* RRM and zinc finger domains is as high as 75% and 73%, respectively.

Specificity of the anti-Caz antibody

We raised a polyclonal antibody against a mixed peptide corresponding to residues 30–45 and 382–390 of *Drosophila* Caz for immunological studies. In order to confirm the specificity of this antibody, we used this anti-Caz polyclonal antibody for immunoblotting analyses of CNS extracts of third instar larvae carrying *elav^{3A}-GAL4/+* (*elav^{3A}/+*, a driver control fly), *UAS-Caz-IR/+* (a responder control fly), and RNAi transgenes encoding inverted repeats corresponding to various Caz regions, *elav^{3A}-GAL4>UAS-Caz-IR* (Figure 2). A single major band with an apparent molecular weight of 45 kDa was detected on immunoblots of all of the flies using the anti-Caz antibody (Figure 2A). Although the size of this protein was slightly larger than the size (38.8 kDa) of the Caz protein predicted based on its amino acid composition, the intensity of this band was significantly reduced in flies carrying *elav^{3A}-GAL4>UAS-Caz-IR$_{1-167}$* (*elav^{3A}/Caz-IR$_{1-167}$*) and those carrying *elav^{3A}-GAL4>UAS-Caz-IR$_{363-399}$* (*Caz-IR$_{363-399}$/+;elav^{3A}/+*) compared with its intensity in either driver control flies (*elav^{3A}/+*) or responder control flies (*UAS-Caz-IR$_{1-167}$/+*) (Figure 2B). There was a significant increase in Caz protein level in CNS extracts from the flies carrying *elav^{3A}/Caz-IR$_{180-346}$* compared with those from control flies carrying *elav^{3A}/+* with unknown causes (Figure 2B). These results indicate that the anti-Caz antibody can specifically detect the Caz protein. These data also confirmed that *Caz* is effectively knocked down in flies carrying *elav^{3A}/Caz-IR$_{1-167}$* and *Caz-IR$_{363-399}$/+;elav^{3A}/+*, but it is not knocked down in flies carrying *elav^{3A}-GAL4>UAS-Caz-IR$_{180-346}$*, which we did not therefore use in the subsequent experiments.

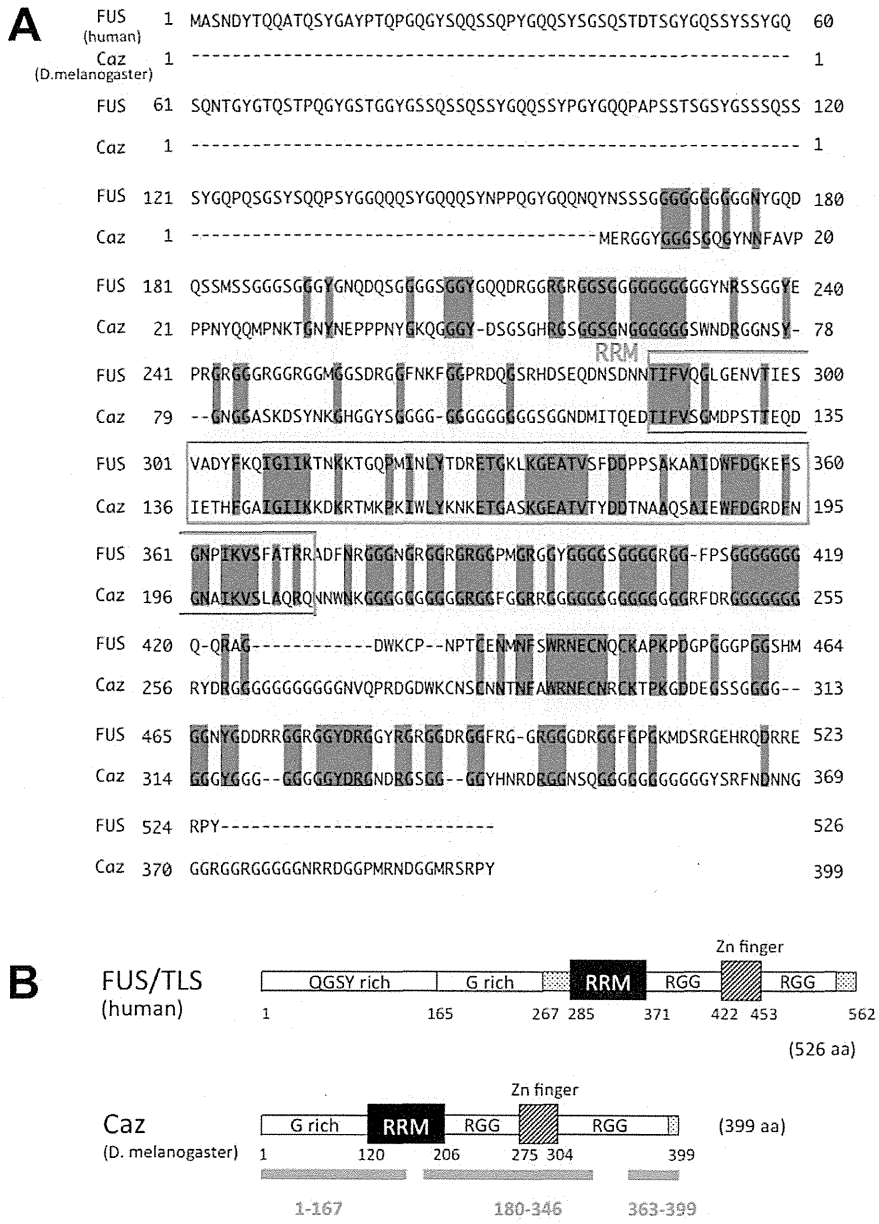

Figure 1. Comparison of human FUS and *Drosophila* Caz. (A) Alignment of human FUS and *Drosophila* Caz amino acid sequences. Identity is indicated in blue. The RNA-recognition-motif (RRM) domain is outlined with a red box. (B) Schematic drawings of domain structures of Human FUS and *Drosophila* Caz proteins. The human FUS protein contains an N-terminal QGSY-rich domain, which functions as a potent transcriptional activation domain [62–64]. The glycine-rich domain (G rich), RRM domain, a domain containing multiple Arg-Gly-Gly (RGG) motifs and a zinc finger (ZnF), are all involved in RNA binding [65,66]. A solid line under the schema of *Drosophila* Caz shows the target genomic sequence of each of the three RNAi transgenes employed in this study, *UAS-Caz-IR*$_{1-167}$, *UAS-Caz-IR*$_{180-346}$ and *UAS-Caz-IR*$_{363-399}$.
doi:10.1371/journal.pone.0039483.g001

The Caz protein is localized in the larval and adult central nervous system of *Drosophila*

The polyclonal anti-Caz antibody was used to examine the expression pattern of the Caz protein in the CNS of third instar *Drosophila* larvae and adult flies (Figure 3). *Drosophila* Caz was strongly expressed in the CNS of both larvae (Figure 3, A1) and adults (Figure 3, E1). No signal was generated in the absence of the primary anti-Caz antibody (Figure 3, D, H) indicating that this signal is specific for detection of the Caz protein. Moreover, the anti-Caz antibody signal did not overlap with the signal of the presynaptic marker Bruchpilot (Brp) that was detected using an anti-Brp antibody (Figure 3, A3-A4, E3-E4). This finding indicates that Caz localizes in a region other than synaptic areas both in third instar larvae and in adult flies (Figure 3, A1-A4, E1-E4), and

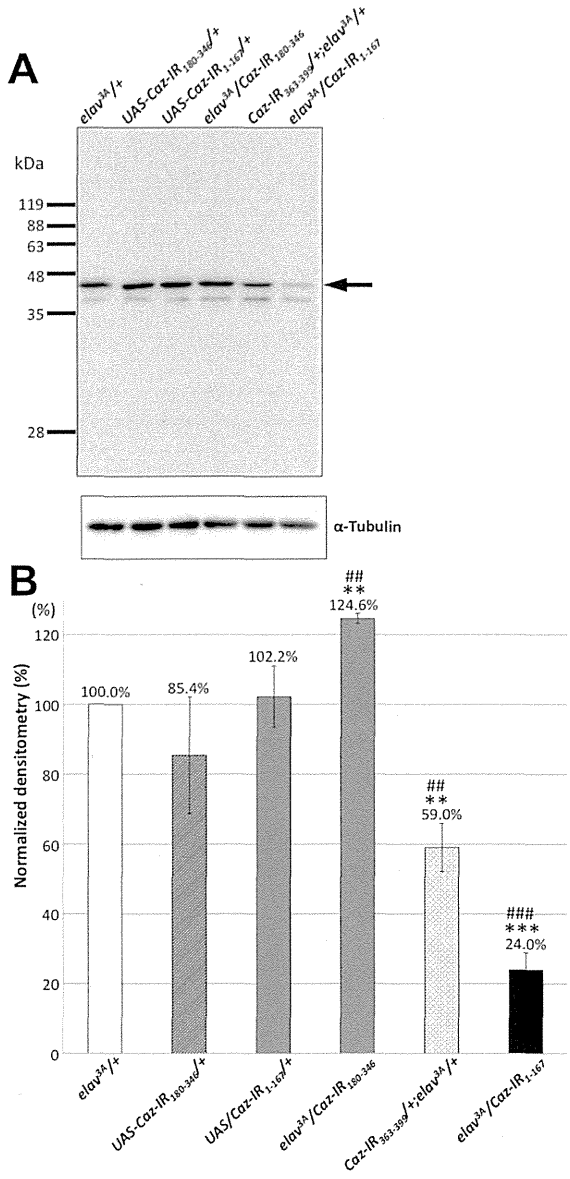

Figure 2. Western immunoblot analysis of the CNS extracts of third instar larvae. (A) A representative result of the analysis of protein extracts from the CNS of the driver control (*elav^{3A}/+*) and responder control (*UAS-Caz-IR$_{180-346}$/+* and *UAS-Caz-IR$_{1-167}$/+*) flies (n = 5, each) and transgenic flies (*elav^{3A}/Caz-IR$_{180-346}$*, *Caz-IR$_{363-399}$/+;elav^{3A}/+* and *elav^{3A}/Caz-IR$_{1-167}$*) (n = 5, each). The blots were probed with the polyclonal anti-Caz antibody that was newly raised for this study. α-Tubulin was used as a loading control. A 45-kDa band (arrow) corresponds to the Caz protein. (B) Densitometric quantification of the 45-kDa bands derived from triplicated immunoblot analyses of the CNS tissues of each fly strain in (A). The intensity of the 45 kDa band which indicates the expression level of Caz protein was much weaker in flies carrying *elav^{3A}/Caz-IR$_{1-167}$* or *Caz-IR$_{363-399}$/+;elav^{3A}/+* than in the driver and responder control flies. The columns and horizontal bars indicate the mean values and the standard errors of the triplicated experiments. **p<0.01 (vs. *elav^{3A}/+*), *** p<0.001 (vs. *elav^{3A}/+*), ##p<0.01 (vs. *UAS-Caz-IR$_{1-167}$/+*), ###p<0.001 (vs. *UAS-Caz-IR$_{1-167}$/+*).
doi:10.1371/journal.pone.0039483.g002

suggests that Caz performs its physiological functions in neuronal cell bodies and/or their axons.

Regarding the precise localization of the Caz protein in neuronal cell bodies, Caz immunoreactivity was detected in the nucleus of neuronal cells of third instar larvae and did not co-localize with actin filaments, which are cytosolic proteins (Figure 4). However, within the nucleus, Caz did not co-localize with diamino-2-phenylidole (DAPI), suggesting that Caz is not localized on chromosomes but is localized in the nucleoplasm (Figure 4, C and D).

Neuron-specific *Caz* knockdown causes fly mobility defects

To analyze the effect of *Caz* knockdown on fly phenotypes, we first investigated whether fly viability was affected by whole-body knockdown of *Caz*. Using an *Act5C-GAL4* driver that expresses GAL4 in the whole body of the fly, we analyzed the phenotypes of flies in which *Caz* double-stranded RNA was expressed throughout the whole body (Table 1). When crossed at 28°C, *UAS-Caz-IR$_{1-167}$* was lethal at the pupal stage for all fly strains that carried it, while the strains carrying *UAS-Caz-IR$_{180-346}$* were viable. When crossed at 25°C to decrease the expression levels of *Act5C-GAL4*, almost all of the strains carrying *UAS-Caz-IR$_{1-167}$*, for which *UAS-Caz-IR$_{1-167}$* had been lethal when crossed at 28°C, changed to be viable.

We next established transgenic fly lines in which *Caz* double-stranded RNA was specifically expressed in neuronal tissue by crossing the transgenic flies with the *elav^{3A}-GAL4* line. As shown above in the immunoblotting analyses of the fly CNS (Figure 2), the expression levels of the Caz protein were much decreased in strain 3 of the fly lines that carried *elav^{3A}/Caz-IR$_{1-167}$* and in the fly line carrying *Caz-IR$_{363-399}$/+;elav^{3A}/+*, compared with the control flies. However, Caz expression levels did not show any detectable decreases in the fly lines carrying *elav^{3A}-GAL4>UAS-Caz-IR$_{180-346}$*. Similar to these results of immunoblotting analyses, immunostaining of the CNS of third instar larvae (Figure 3, B1, C1) and adult flies (Figure 3, F1, G1) showed that immunoreactivity detected with the anti-Caz antibody also decreased in the CNS tissues derived from the fly lines carrying *elav^{3A}/Caz-IR$_{1-167}$* (strain 3) (Figure 3, B1: larva, F1: adult fly) and *Caz-IR$_{363-399}$/+;elav^{3A}/+* (Figure 3, C1: larva, G1: adult fly). These results confirmed that *Caz* is effectively knocked down in the CNS of those two lines of transgenic flies.

To examine the effects of neuron-specific *Caz*-knockdown on the fly life span, we next determined the life span of each genotype (Figure 5). We examined adult flies until 120 days after eclosion, but there were no significant differences in life span between the control flies carrying *elav^{3A}/+* (n = 145) and those carrying *elav^{3A}/Caz-IR$_{1-167}$* (n = 144) or *Caz-IR$_{363-399}$/+;elav^{3A}/+* (n = 161), in which the CNS expression of Caz was efficiently knocked down (Figure 5). The average life span of the control flies was 73.9 days, whereas flies carrying *elav^{3A}/Caz-IR$_{1-167}$* and *Caz-IR$_{363-399}$/+;elav^{3A}/+* lived an average of 76.5 days and 70.7 days, respectively. Fly life spans were therefore not significantly different between the control and neuron-specific *Caz*-knockdown flies.

In order to further evaluate the functional effects of neuron-specific *Caz* knockdown, we then performed climbing assays of the *Caz*-knockdown fly strains (Figure 6). The flies carrying *elav^{3A}/Caz-IR$_{1-167}$* showed reduced mobility both on day 3 (−10.7%) and day 21 (−9.3%) compared to the control flies carrying *elav^{3A}/+*. Similarly *Caz-IR$_{363-399}$/+;elav^{3A}/+* carrying flies showed reduced mobility both on day 3 (−5.1%) and on day 21 (−10.6%). All of these reductions in mobility were statistically significant (p<0.001). These results indicate that *Caz* is involved in locomotion.

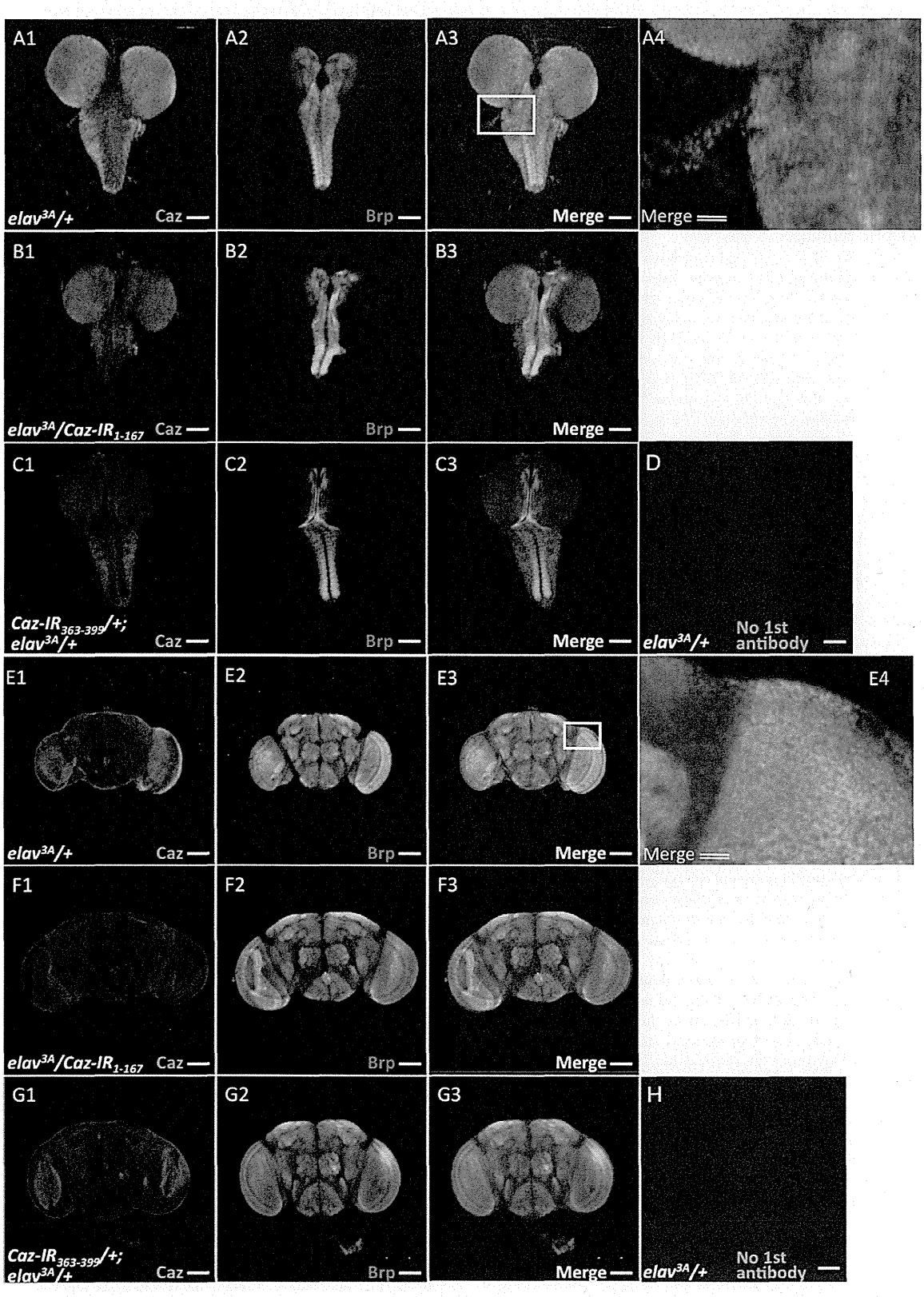
A1
elav3A/+
Caz
A2
Brp
A3
Merge
A4
Merge
B1
elav3A/Caz-IR1-167
Caz
B2
Brp
B3
Merge
C1
Caz-IR363-399/+;
elav3A/+
Caz
C2
Brp
C3
Merge
D
elav3A/+
No 1st
antibody
E1
elav3A/+
Caz
E2
Brp
E3
Merge
E4
Merge
F1
elav3A/Caz-IR1-167
Caz
F2
Brp
F3
Merge
G1
Caz-IR363-399/+;
elav3A/+
Caz
G2
Brp
G3
Merge
H
elav3A/+
No 1st
antibody

Figure 3. Immunohistochemical localization of Caz in larval and adult brains. Brain-ventral ganglia complexes from third instar larvae (A–D) and whole mount adult heads (E–H) were stained with the polyclonal anti-Caz antibody (A-1, B-1, C-1, E-1, F-1, G-1) or with an antibody against the neuropil marker Bruchpilot (Brp) (A-2, B-2, C-2, E-2, F-2, G-2). Merged confocal images of the two stains are shown at right (A-3, B-3, C-3, E-3, F-3 and G-3, respectively). Higher-magnification images of the boxed area in A-3 and E-3 are shown in A-4 and E-4, respectively. (D, H) Images of staining in the absence of first antibody. A-1 to A-4, E-1 to E-4, controls carrying $elav^{3A}$/+; B-1 to B-3, F-1 to F-3, *Caz*-knockdown flies carrying $elav^{3A}$/*Caz-IR*$_{1-167}$; C-1 to C-3, G-1 to G-3, *Caz*-knockdown flies carrying *Caz-IR*$_{363-399}$/+;$elav^{3A}$/+. Caz antibody immunoreactivity decreased in CNS tissues from both the third instar larvae and the adult flies carrying $elav^{3A}$/*Caz-IR*$_{1-167}$ (B-1, F-1) and *Caz-IR*$_{363-399}$/+;$elav^{3A}$/+ (C-1, G-1). The single bars indicate 100 μm. The double bars indicate 20 μm.
doi:10.1371/journal.pone.0039483.g003

Caz regulates the formation of motoneurons at presynaptic terminals in the NMJ

Based on the fact that *Caz*-knockdown flies showed motor deficits in the climbing assays, together with the fact that *FUS*, the human counterpart of *Caz*, is involved in ALS that impairs motor neurons, we therefore decided to analyze the morphology of motoneuron presynaptic terminals at NMJs in these flies. Because most motoneurons of the adult fly originate from larval motoneurons, we compared the NMJ structure of the larvae of $elav^{3A}$/*Caz-IR*$_{1-167}$ and *Caz-IR*$_{363-399}$/+;$elav^{3A}$/+ flies with that of larvae of control flies carrying $elav^{3A}$/+ or *UAS-Caz-IR*$_{363-399}$/+. None of these *Caz*-knockdown fly larvae showed apparent changes in NMJ structure (Figure 7, A-D). However, measurement of the total length of synaptic branches of motoneurons in these larvae indicated that the total branch length was significantly decreased in $elav^{3A}$/*Caz-IR*$_{1-167}$ (75.3±11.9 μm) and *Caz-IR*$_{363-399}$/+;$elav^{3A}$/+ (75.3±19.5 μm) flies compared to that of the both driver ($elav^{3A}$/+; 94.8±19.9 μm) and responder (*UAS-Caz-IR*$_{363-399}$/+; 105.4±17.5 μm) control *flies*. (Figure 7, E). The flies carrying $elav^{3A}$/*Caz-IR*$_{1-167}$ showed the significantly decreased number of the synaptic boutons (9.3±2.1) compared to the both driver (15.9±4.5) and responder (17.1±4.7) control flies, and so did the flies carrying *Caz-IR*$_{363-399}$/+;$elav^{3A}$/+ (11.8±5.6) compared to the responder controls (Figure 7, F). There were no significant differences in the size of synaptic boutons among those 4 genotypes (Figure 7, G). These results indicate that Caz is required for synaptic terminal growth at the NMJ.

Discussion

We showed here that *Drosophila* Caz is strongly expressed in the central nervous system of larvae and adults. Caz did not colocalize with the presynaptic protein Brp, suggesting that Caz performs its physiological functions in neuronal cell bodies and/or their axons. In order to clarify whether or not disruption of the physiological functions of Caz are critical for the development of neurodegeneration even in the absence of abnormal Caz aggregates, we established fly models in which the *Caz* gene, which is the *Drosophila* FUS homologue, was knocked down. We demonstrated that neuron-specific knockdown of *Caz* did not affect the life span of the *Caz*-knockdown flies but did reduce the climbing abilities of adult flies, and also caused anatomical defects in presynaptic terminals of motoneurons in third instar larvae. These results suggested that a decrease in *Caz* expression is sufficient for the development of defects in locomotive abilities and for a decrease in the total length of synaptic branches of motoneurons at the NMJs in this *Drosophila* model. These data may indicate that the loss of physiological FUS functions in motoneurons would be more fundamental than the formation of cytoplasmic FUS aggregates in the pathogenesis of human FUS-related ALS/FTLD.

To eliminate the possibility that off-target effects of our RNAi construct that contained inverted repeats might generate the observed phenotypes, we used two different Caz inverted repeat constructs (*UAS-Caz-IR*$_{1-167}$ and *UAS-Caz-IR*$_{363-399}$) whose target sequences did not overlap with each other. We established four transgenic fly strains carrying *UAS-Caz-IR*$_{1-167}$ as listed in Table 1. We also obtained a fly strain carrying *UAS-Caz-IR*$_{363-399}$ from the Vienna *Drosophila* RNAi center (VDRC). This fly strain carries an RNAi that is targeted to the region corresponding to residues 363-399 of *Drosophila* Caz (*UAS-Caz-IR*$_{363-399}$), We then crossed these transgenic flies with the $elav^{3A}$-*GAL4* line to specifically express *Caz* double stranded RNA in neuronal tissues. Each independent fly strain carrying $elav^{3A}$/*Caz-IR*$_{1-167}$ showed essentially the same phenotype as the strain carrying *Caz-IR*$_{363-399}$/+;$elav^{3A}$/+. These results suggest that the phenotypes observed in the neuron-specific Caz-knockdown flies were not due to an off-target effect but rather to a reduction in Caz protein levels.

Mutations in the *FUS* gene are associated with inherited forms of both ALS and FTLD [15,16,18,19]. The *FUS* gene was originally identified in a study that found that the FUS protein forms part of a fusion protein with the transcription factor CHOP, which arises due to a chromosomal translocation in liposarcoma [26]. It has been reported that there are both dominantly and recessively inherited families of ALS with *FUS* mutations [15]. Before the discovery of these *FUS* mutations in familial ALS, mutations in the *TARDBP* gene that encodes another RNA-binding protein, TDP-43, had been reported to be associated with familial ALS and FTLD [7-14]. Both the *FUS* gene and the *TARDBP* gene encode an RNA-binding protein equipped with an RRM, and should therefore be involved in RNA processing, splicing, and RNA metabolism. Since FUS and TDP-43 have substantial similarities in their protein structure and putative functions, they could therefore cause ALS or FTLD through common pathogenic processes [2,38]. However, the mechanisms through which mutations in *FUS* or *TARDBP* cause ALS and FTLD are not known, and both toxic gain-of-function and loss-of-function models have been proposed [2,38]. ALS-associated mutant forms of TDP-43 and FUS are known to form abnormal cytosolic aggregates [15,16,35,39–41], and high-level overexpression of either wild-type or mutant TDP-43 is neurotoxic in mice, zebra fish and *Drosophila* [42–47]. One recent study reported that a *Drosophila* model in which targeted expression of mutant human FUS in *Drosophila* motor neurons led to locomotor dysfunction [48]. These findings would support the toxic gain-of-function model. However, overexpression of mutant proteins may also perturb the activity of endogenous TDP-43, supporting the loss-of-function model [49]. Similarly, the targeted expression model mentioned above reported that deletion of the nuclear export signal rescued toxicity associated with mutant FUS, suggesting that delocalization of FUS from the nucleus to the cytoplasm, namely the loss-of-nuclear-function, would be necessary for neurodegeneration [48]. In this study, we demonstrated that neuron-specific knockdown of *Caz*, the *Drosophila FUS* homologue, could induce a defect in fly locomotive abilities as well as degeneration of motoneurons at NMJs in the model flies. There has been one previous report that showed that flies lacking TBPH, the *Drosophila* TDP-43 homologue, present deficient locomotive behaviors, reduced life span and anatomical defects at the NMJs [37]. Regarding *FUS* and its homologues, one recent study reported that *Drosophila* mutants in which the *Caz* gene was disrupted exhibited

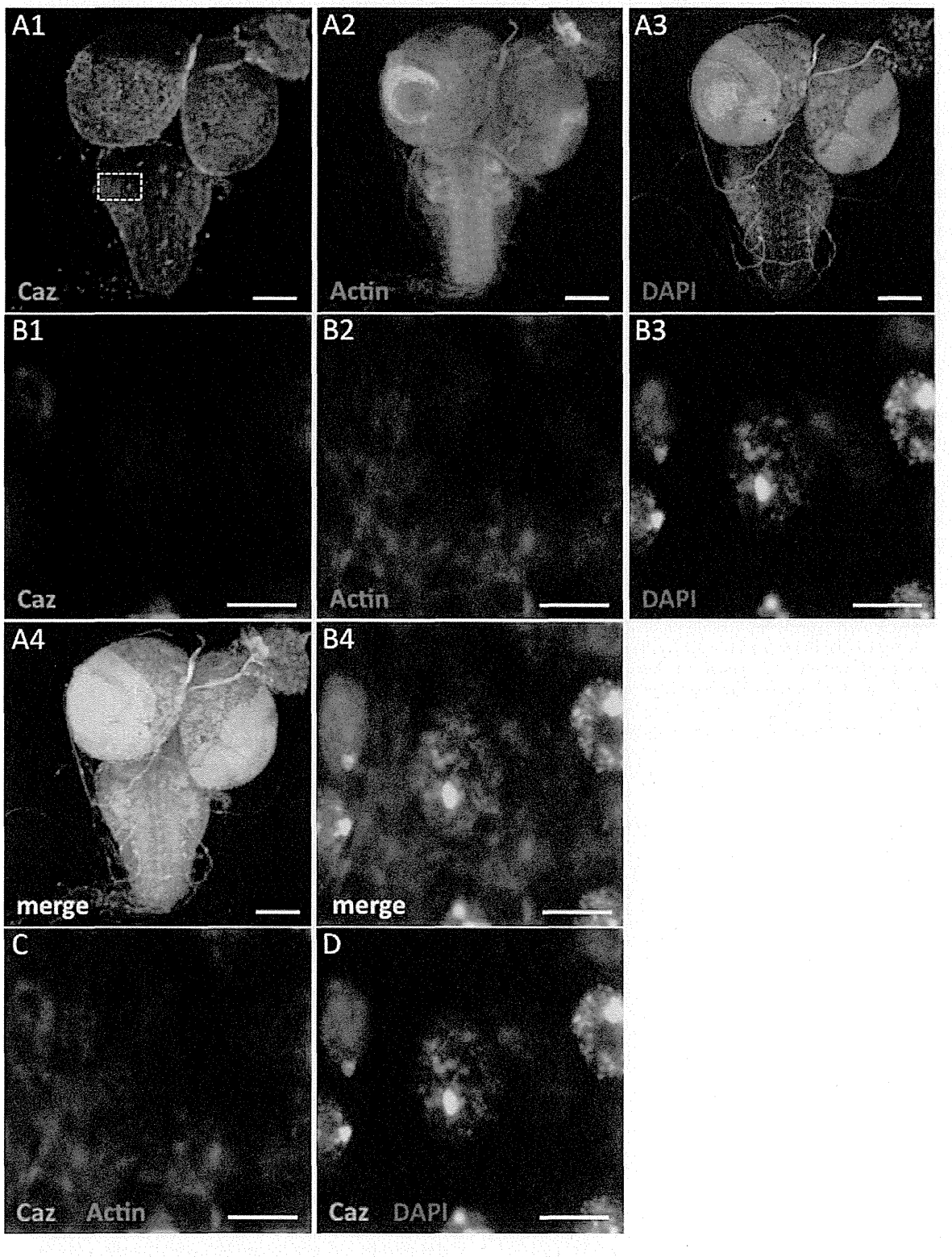

Figure 4. Intraneuronal localization of Caz in larval brains. Brain-ventral ganglia complexes from third instar larvae (A–D) were stained with the anti-Caz antibody (A-1, B-1), diamino-2-phenylidole (DAPI) (nuclear staining; A-2, B-2) or phalloidin (F-actin staining; A-3, B-3). Panels B-1 to B-4 are higher magnification images of the boxed area in A-1. Merged confocal images of A-1 to A-3, B-1 to B-3, B-1 and B-2, and B-1 and B-3 are shown in A-

4, B-4, C, and D, respectively. The bar indicates 100 μm (A) or 5 μm (B–D). Anti-Caz antibody-immunoreactivity was detected in the nucleus of neuronal cells and did not co-localize with actin filaments, which stained with phalloidin. Since Caz did not co-localize with DAPI, which stains chromosomes, Caz must therefore localize in the nucleoplasm.
doi:10.1371/journal.pone.0039483.g004

decreased adult viability, diminished locomotor speed and reduced life span compared with controls, and that these phenotypes were fully rescued by wild-type human *FUS*, but not by ALS-associated mutant *FUS* [50]. These reports, together with our results, demonstrated that a lack of physiological functions of FUS or TDP-43 in the nucleus is sufficient for induction of locomotive dysfunction and motoneuron degeneration, which recapitulate the phenotypes of ALS, and they therefore imply that the loss of physiological FUS functions are sufficient for the development of pathogenic processes similar to those that occur in FUS- or TDP-43-related ALS/FTLD, in the absence of cytosolic aggregates that may be toxic to motoneurons in ALS/FTLD.

There have been a few previous studies in which loss-of-function animal models of FUS-related human disorders were generated. FUS knockout mice show perinatal lethality and defects in B lymphocyte development [51]. Additionally, the hippocampal pyramidal neurons of these FUS-null mice exhibited abnormal spine morphology and lower spine density [52]. One report showed that surviving knockout mice exhibited male sterility [53]. However, the neurodegenerative phenotypes of these mice have not been reported to date. With regard to *Drosophila* models, one recent paper that was mentioned above presented a mutant fly strain (named the *Caz1* mutant) in which 58% of the *Caz* gene was deleted by creating a small genomic deletion [50]. This fly model developed a phenotype of disturbed locomotion that is similar to that observed in the *Caz*-knockdown flies in the present study. The differences between the *Caz1* mutant and our fly models were as follows; 1) the *Caz1* mutant did not show any morphological abnormalities at the NMJs i.e., shortening of the presynaptic terminals of motoneurons and decrease in the number of synaptic boutons, both of which were observed in our *Caz*-knockdown models. 2) The *Caz1* mutant showed reduced life spans, which were not observed in our models, and this life-span defect of *Caz1* mutant could be fully rescued by expression of wild-type fly *Caz* or wild-type human *FUS* in neurons using *elav-Gal4*. The difference in life span between the *Caz1* mutant and our *Caz*-knockdown models might be caused by differences in the expression pattern of the transgenes between the two models; in our fly models *Caz* gene expression was knocked down specifically in the nervous system, whereas, in the short-lived *Caz1* mutant flies, *Caz* was disrupted throughout the whole body. In our *Caz*-knockdown models, the expression of Caz protein was knocked down to 40–60% in the CNS (Figure 2), but their life spans were not reduced. Together with the fact that the reduced life span of the *Caz1* mutant was rescued by the neuronal expression of wild-type *Caz*, our results suggest that substantial expression of *Caz* in neuronal tissues, even though it is not fully expressed, could sufficiently keep their life spans within normal range. Our model flies also demonstrated that normal expression of *Caz* in neurons is essential for the elongation of synaptic branches of motoneurons at NMJs, and therefore that *Caz*-knockdown would induce impaired maturation of these synaptic branches, resulting in the observed locomotive deficit in our model flies, in the absence of any non-neuronal effect of the Caz protein.

In conclusion, we established fly models with neuron-specific knockdown of the *Drosophila* FUS homologue, and showed that those flies developed locomotive deficits as well as anatomical defects of motoneurons at NMJs. Our results indicate that the loss

Table 1. Established fly strains carrying *UAS-Caz-IR*.

Transgene	Strain	Chromosome linkage	Act5C-GAL4>		elav^{3A}-GAL4>
			28°C	25°C	
UAS-Caz-IR$_{1-167}$	3	III	lethal	lethal	LD (+)
	4	III	lethal	NE	ND
	11	II	lethal	NE	ND
	21	III	lethal	NE	ND
UAS-Caz-IR$_{180-346}$	11	II	NE	NE	NE
	12	II	NE	NE	NE
	17	II	NE	NE	ND
	22	III	NE	ND	LD (−)
	24	III	NE	NE	LD (−)
	32	III	ND	ND	ND
	33	III	ND	NE	ND
UAS-Caz-IR$_{363-399}$		II	NE	ND	LD (+)

LD: locomotive dysfunction, NE: no effect, ND: not determined.
doi:10.1371/journal.pone.0039483.t001

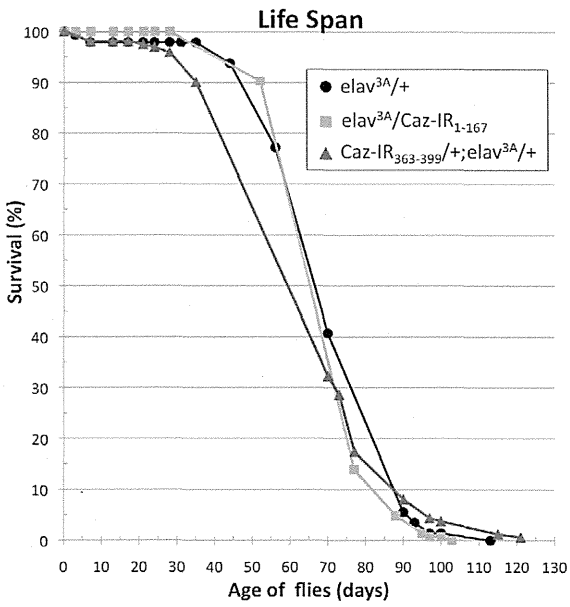

Figure 5. Life-span analyses of flies of each genotype. Percentage survival of adult male flies of the indicated genotypes is shown. Flies were collected from 20 different batches. The total number of flies counted was: *elav^{3A}/+* (n = 145), *elav^{3A}/Caz-IR$_{1-167}$* (n = 144) and *Caz-IR$_{363-399}$/+;elav^{3A}/+* (n = 161). There were no significant differences in the life span of flies with the indicated genotypes.
doi:10.1371/journal.pone.0039483.g005

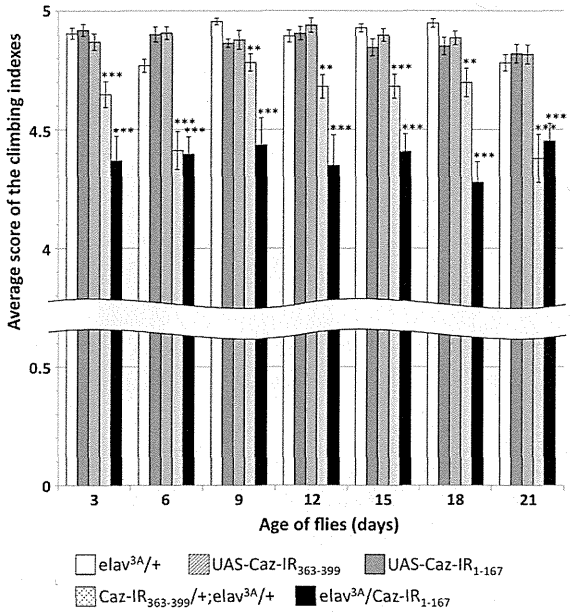

Figure 6. Climbing assays. Five independent tests were performed for each genotype. The total number of flies counted was: *elav^{3A}/+* (a driver control, n = 309), *UAS-Caz-IR$_{363-399}$/+* (a responder control, n = 222), *UAS-Caz-IR$_{1-167}$/+* (a responder control, n = 246), *Caz-IR$_{363-399}$/+;elav^{3A}/+* (n = 265) and *elav^{3A}/Caz-IR$_{1-167}$* (n = 238). There was no significant difference in climbing abilities between the driver and responder control flies in each day after eclosion. Flies carrying *elav^{3A}/Caz-IR$_{1-167}$* or *Caz-IR$_{363-399}$/+;elav^{3A}/+* showed a significantly reduced ability to climb upwards compared to *elav^{3A}/+* flies in each examined day. The horizontal bars indicate standard errors of mean values. ***p<0.001, **p<0.005.
doi:10.1371/journal.pone.0039483.g006

of physiological FUS functions in the nucleus is more likely to be the fundamental pathogenic mechanism that causes FUS-related ALS/FTLD than the toxicity of cytoplasmic aggregates. These data further indicate future research directions, suggesting that it will be necessary to identify target molecules, including nuclear proteins and/or RNA species that associate with FUS, in order to elucidate the molecular mechanisms leading to neuronal dysfunction in FUS-associated ALS/FTLD and to develop the disease-modifying therapies that are eagerly desired in those relentless neurodegenerative diseases. In any event, the *Drosophila* model that we established in the present study, which recapitulates key features of human ALS, would be suitable for the screening of genes and chemicals that can modify these pathogenic processes that lead to the degeneration of motoneurons in ALS.

Materials and Methods

Fly stocks

Fly stocks were maintained at 25°C on standard food containing 0.7% agar, 5% glucose and 7% dry yeast. Canton S was used as the wild type. W; *UAS-Caz-IR*; + (CG3606) was obtained from the Vienna *Drosophila* RNAi center (VDRC). The RNAi of this strain was targeted to the region corresponding to residues 363-399 of *Drosophila* Caz (*UAS-Caz-IR$_{363-399}$*). P{*GAL4-elav.L*}3A (elav^{3A}-GAL4) was provided by Dr. Bryan Stewart [54]. The Act5C-GAL4 strain was obtained from the Bloomington *Drosophila* stock center. Establishment of the lines carrying GMR-GAL4 was as described previously [55].

Comparison of amino acid sequences of human FUS and *Drosophila* Caz

The amino acid sequence of *Drosophila* Caz was retrieved from the Flybase (http://flybase.org). The identity and the similarity of *Drosophila* Caz and human FUS were compared using BLAST (http://blast.genome.jp/) and FASTA (http://fasta.genome.jp/). FASTA was used for comparison of the entire sequences, and BLAST was used for comparison of each corresponding domain between Caz and FUS.

Establishment of the transgenic flies

To establish transgenic fly lines carrying *UAS-Caz-IR*, 500-bp fragments of Caz ORFs (*UAS-Caz-IR$_{1-167}$*; 5′-ATGGAACGTGGCGGTTATGGTGGT to 5′-AGAACAAGGAGACCGGCGC, *UAS-Caz-IR$_{180-346}$*; 5′-ATGCTGCACAATCCGCCATTGAAT to 5′-CAACAGAGATCGCGGTGGC) from *Caz* cDNA clone CG3606 were amplified, and then individually cloned into the pENTR/D-TOPO vector (Invitrogen Life Technologies Japan Corporation, Tokyo, Japan), in which each trigger sequence of *Caz* was placed between the *attL1* and *attL2* recombination sequences. Following confirmation by sequencing, two copies of each trigger sequence were transferred into the pRISE transformation vector that contains a characteristic inverted repeat of *attR1-cm^r-ccdB-attR2* in a recombination cassette by an *in vitro* reaction mediated by LR Clonase (Invitrogen), a DNA recombinase that specifically recognizes the *attL* and *attR2* target sites [56]. Due to the recombination reaction between the *attL* and *attR2* sites, the ccdB sequence was replaced by the target cDNA, resulting in the cloning of a head-to-head inverted repeat (IR) of Caz into the plasmid.

These plasmids were verified by sequencing and then injected into embryos to obtain stable transformant lines carrying *UAS-Caz-IR*. P element-mediated germ line transformation was carried out as described previously [57], and F1 transformants were selected on the basis of white-eye color rescue [58]. Four and seven transgenic strains carrying *UAS-Caz-IR$_{1-167}$* and *UAS-Caz-IR$_{180-346}$* were established, respectively (responder controls), as listed in Table 1. To drive expression of *Caz* double stranded RNA in the whole body of the flies or specifically in neuronal tissues, we crossed the transgenic flies with either the *Act5C-GAL4* line or the *elav^{3A}-GAL4* line (*elav^{3A}-GAL4/+*; a driver control). Each transgenic strain showed a consistent phenotype (Table 1).

Production of rabbit anti-Caz antibodies

Rabbit anti-Caz antibodies were produced by MEDICAL & BIOLOGICAL LABORATORIES Co., Ltd (MBL, Ina, Japan). The peptides, N-NKTGNYEPPPNYGKQGC-C (residues 29–45; the underlined C residue C was an added residue) and N-CRDGGPMRNDGGMRSRPY-C (residues 383–399), which correspond respectively to the N- and C-terminal sequences of Caz, were individually conjugated with KLH (Keyhole limpet hemocyanin). These two KLH-conjugated peptides were mixed with Freund's complete adjuvant to provide a suspension, which was injected intradermally into rabbits (Female Japanese White). The rabbits were then boosted with inoculations of an immunogen of the same quality once a week for 7 weeks, and a terminal bleed was performed to collect the maximum amount of serum. The serum was purified by affinity chromatography against the synthesized peptides using a Protein G column.

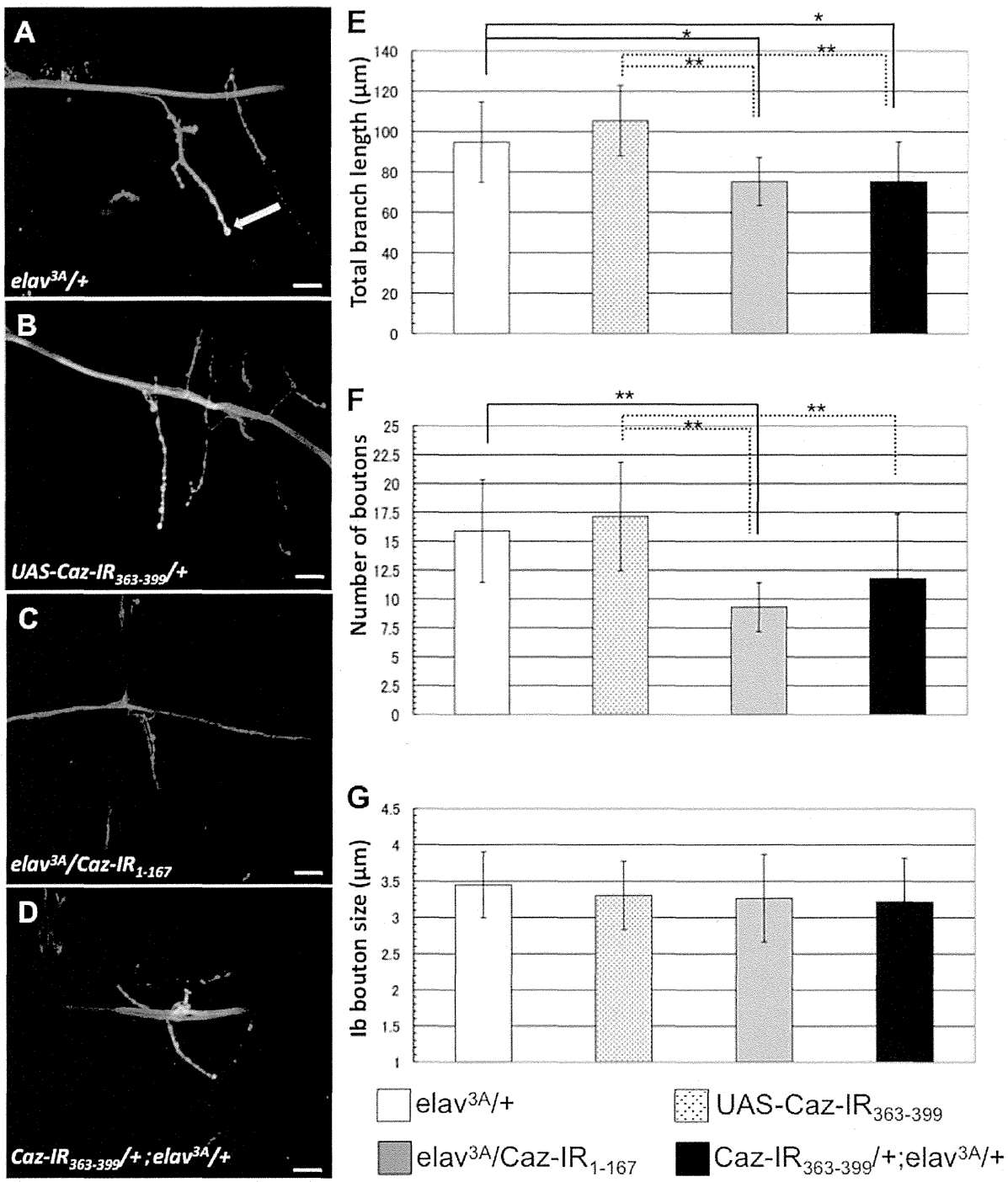

Figure 7. Confocal images of anti-HRP staining of muscle 4 synapses in third instar larvae. A representative image of the indicated genotypes is shown; (A) *elav*^{3A}/+ (a driver control), (B) *UAS-Caz-IR*$_{363\text{-}399}$/+ (a responder control), (C) *elav*^{3A}/*Caz-IR*$_{1\text{-}167}$ and (D) *Caz-IR*$_{363\text{-}399}$/+;*elav*^{3A}/+. The bar indicates 20 μm. (E) Total branch length of the NMJ from muscle 4 for each of the indicated genotypes. n = 9 for each genotype. (F, G) The number (F) and the size (G) of the synaptic boutons for each of the indicated genotypes. (F) n = 9 for each genotype. (G) The size of Ib bouton (indicated with an arrow in A) was measured. n = 30 for *elav*^{3A}/+, n = 34 for *Caz-IR*$_{363\text{-}399}$/+, n = 27 for *elav*^{3A}/*Caz-IR*$_{1\text{-}167}$, n = 34 for *Caz-IR*$_{363\text{-}399}$/+*elav*^{3A}/+. The *Caz*-knockdown flies did not show any apparent changes in NMJ structure. However, the total length of synaptic branches of the motoneurons was significantly decreased in each Caz-knockdown fly strain (*elav*^{3A}/*Caz-IR*$_{1\text{-}167}$ and *Caz-IR*$_{363\text{-}399}$/+;*elav*^{3A}/+) compared to the both driver and responder control flies (E). The flies carrying *elav*^{3A}/*Caz-IR*$_{1\text{-}167}$ showed the significantly decreased number of the synaptic boutons compared to the

both driver and responder control flies, and so did the flies carrying *Caz-IR$_{363-399}$/+;elav^{3A}/+* compared to the responder controls (F). There were no significant differences in the size of synaptic boutons among those 4 genotypes (G). The horizontal bars indicate standard errors of mean values. *p<0.05, **p<0.01.
doi:10.1371/journal.pone.0039483.g007

Immunoblotting analysis

Protein extracts from the central nervous system (CNS) of *Drosophila* carrying *elav^{3A}-GAL4/+*, *UAS-Caz-IR$_{180-346}$/+*, *UAS-Caz-IR$_{1-167}$/+* and *elav^{3A}-GAL4>UAS-Caz-IR* were prepared as previously described [59]. Briefly, the CNS was excised from third instar larvae and homogenized in a sample buffer containing 50 mM Tris-HCl (pH 6.8), 2% SDS, 10% glycerol, 0.1% bromophenol blue and 1.2% β-mercaptoethanol. The homogenates were boiled at 100°C for 5 min, and then centrifuged. The supernatants (extracts) were electrophoretically separated on SDS-polyacrylamide gels containing 12% acrylamide and then transferred to polyvinylidene difluoride (PVDF) membranes (Bio-Rad, Osaka, Japan). The blotted membranes were blocked with TBS/0.05% Tween containing 5% skim milk for 1 h at 25°C, followed by incubation with rabbit polyclonal anti-Caz at a 1:5,000 dilution for 16 h at 4°C. After washing, the membranes were incubated with HRP-conjugated anti-rabbit IgG (GE Healthcare Bioscience, Tokyo, Japan) at 1:10,000 dilution for 2 h at 25°C. Antibody binding was detected using ECL Western blotting detection reagents (GE Healthcare Bioscience) and images were analyzed using a Lumivision Pro HSII image analyzer (Aisin Seiki, Kariya, Japan). To ensure equal protein loading in each lane, the membranes were also probed with an anti-α-tubulin antibody after stripping the complex of anti-Caz antibody and HRP-conjugated anti-rabbit IgG. For the detection of α-tubulin, mouse anti-α-tubulin monoclonal antibody (1:5,000 dilution, Sigma, Tokyo, Japan) and an HRP-conjugated anti-mouse IgG (1:10,000 dilution, GE Healthcare Bioscience) were used as the primary and secondary antibodies, respectively.

Immunostaining

For immunohistochemical analysis, CNS tissues of third instar larvae and adult flies were dissected, and fixed in 4% paraformaldehyde/PBS for 15 min at 25°C. After washing with PBS containing 0.3% Triton X-100, the samples were blocked with blocking buffer (PBS containing 0.15% Triton X-100 and 10% normal goat serum) for 30 min at 25°C, and then incubated with diluted primary antibodies in the blocking buffer for 20 h at 4°C. The following antibodies were used; 1:1,000 diluted rabbit anti-Caz antibody and 1:100 diluted mouse anti-Brp antibody (Developmental Studies Hybridoma Bank [DSBH] nc82). After extensive washing with PBS containing 0.3% Triton X-100, samples were incubated with secondary antibodies labeled with either Alexa 546 or Alexa 488 (1:400; Invitrogen) diluted in the blocking buffer, in the dark, for 2 h at 25°C. After extensive washing with PBS containing 0.3% Triton X-100 and PBS, samples were mounted in Fluoroguard Antifade Reagent (Bio-Rad) and observed under a Zeiss LSM510 confocal laser scanning microscope.

For NMJ staining, third instar larvae were dissected in HL3 saline [60] and fixed in 4% paraformaldehyde/PBS for 30 min. The blocking buffer was 2% bovine serum albumin (BSA)/PBS/0.1% TritonX-100. FITC-conjugated goat anti-HRP (1:1,000, MP Biochemicals) was used as the detection antibody. The samples were mounted and observed under a Zeiss LSM510 confocal laser scanning microscope. MN4 (Ib) in muscle 4 in abdominal segment 2 was quantified. Images were acquired using a Zeiss LSM510 by merging 1 μm interval z-sections onto a single plane. Nerve terminal branch lengths were measured using Image J software.

To determine whether Caz is present in the nucleus or not, CNS tissues of third instar larvae were dissected, and fixed in 4% paraformaldehyde/PBS for 15 min at 25°C. After washing with PBS containing 0.3% Triton X-100, the samples were incubated with Alexa 488-conjugated phalloidin (1 unit/200 μl) in PBS containing 0.3% Triton X-100 for 20 min at 25°C. The samples were then blocked and reacted with the primary and the secondary antibodies as described for the immunohistochemical analysis described above, except that the mouse anti-Brp antibody was not used. After extensive washing with PBS containing 0.3% Triton X-100, the samples were stained with DAPI (0.5 μg/ml)/PBS/0.1% Triton X-100. Following washing with PBS containing 0.1% Triton X-100 and PBS, the samples were mounted and observed under a confocal laser scanning microscope (OLYMPUS Fluoview FV10i).

Longevity assay

Longevity assays were carried out in a humidified, temperature controlled incubator at 25°C and 60% humidity on a 12-h light and 12-h dark cycle on standard fly food. Flies carrying *elav^{3A}-GAL4/+* and *elav^{3A}-GAL4>UAS-Caz-IR* were placed at 28°C, and newly eclosed adult flies were separated and placed in vials at a low density (10–20 flies per vial) with a male: female ratio of 1: 1. Every 3 days, they were transferred to new tubes containing fresh food and deaths were scored. Survival rate was determined by plotting a graph of the percentage of surviving flies versus days.

Climbing assay

Climbing assays were performed as described previously [61]. Flies carrying *elav^{3A}-GAL4/+*, *UAS-Caz-IR$_{363-399}$/+*, *UAS-Caz-IR$_{1-167}$/+*, and *elav^{3A}-GAL4>UAS-Caz-IR* were placed at 28°C, and newly eclosed adult flies were separated and placed in vials at a density of 30 flies per vial (15 males and 15 females). Flies were transferred, without anesthesia, to a conical tube. The tube was tapped to collect the flies to the bottom, and they were then given 30 s to climb the wall. After 30 s the flies were collected at the bottom by tapping of the tube, and were again allowed to climb for 30 s. Similar procedures, all of which were videotaped, were repeated five times in total. For all of the climbing experiments, the height to which each fly climbed was scored as follows (score (height climbed)); 0 (less than 2 cm), 1 (between 2 and 3.9 cm), 2 (between 4 and 5.9 cm), 3 (between 6 and 7.9 cm), 4 (between 8 and 9.9 cm) and 5 (greater than 10 cm). The climbing index of each fly strain was calculated as follows; the sum of the products of each score multiplied by the number of flies for which that score was recorded, was calculated, and this number was then divided by five times the total number of flies examined. These climbing assays were carried out every 3 days until the 18th day after eclosion.

Data analysis

All statistical analyses were performed using Microsoft Excel. The Mann-Whiney test was used for assessment of the statistical significance of comparisons between groups of data concerning median life span. For other assays the two-way ANOVA was used to determine the statistical significance of comparisons between groups of data. When the two-way ANOVA showed significant

variation among the groups, Dunnet's test was subsequently used for pairwise comparisons of groups. All data are shown as means ± SEM.

Author Contributions

Conceived and designed the experiments: TT MY MN TY TM. Performed the experiments: HS MS YA MY. Analyzed the data: TT HS MS MY. Contributed reagents/materials/analysis tools: NF YN MN. Wrote the paper: TT MS HS MY.

References

1. Boillée S, Vande Velde C, Cleveland DW (2006) ALS: a disease of motor neurons and their nonneuronal neighbors. Neuron 52: 39–59.
2. Mackenzie IR, Rademakers R, Neumann M (2010) TDP-43 and FUS in amyotrophic lateral sclerosis and frontotemporal dementia. Lancet Neurol 9: 995–1007.
3. Lomen-Hoerth C, Anderson T, Miller B (2002) The overlap of amyotrophic lateral sclerosis and frontotemporal dementia. Neurology 59: 1077–1079.
4. Murphy JM, Henry RG, Langmore S, Kramer JH, Miller BL, et al. (2007) Continuum of frontal lobe impairment in amyotrophic lateral sclerosis. Arch Neurol 64: 530–534.
5. Neumann M, Sampathu DM, Kwong LK, Truax AC, Micsenyi MC, et al. (2006) Ubiquitinated TDP-43 in frontotemporal lobar degeneration and amyotrophic lateral sclerosis. Science 314: 130–133.
6. Arai T, Hasegawa M, Akiyama H, Ikeda K, Nonaka T, et al. (2006) TDP-43 is a component of ubiquitin-positive tau-negative inclusions in frontotemporal lobar degeneration and amyotrophic lateral sclerosis. Biochem Biophys Res Commun 351: 602–611.
7. Gitcho MA, Baloh RH, Chakraverty S, Mayo K, Norton JB, et al. (2008) TDP-43 A315T mutation in familial motor neuron disease. Ann Neurol 63: 535–538.
8. Yokoseki A, Shiga A, Tan CF, Tagawa A, Kaneko H, et al. (2008) TDP-43 mutation in familial amyotrophic lateral sclerosis. Ann Neurol 63: 538–542.
9. Lacomblez L, Pochigaeva K, Salachas F, Pradat PF, Camu W, et al. (2008) TARDBP mutations in individuals with sporadic and familial amyotrophic lateral sclerosis. Nat Genet 40: 572–574.
10. Sreedharan J, Blair IP, Tripathi VB, Hu X, Vance C, et al. (2008) TDP-43 mutations in familial and sporadic amyotrophic lateral sclerosis. Science 319: 1668–1672.
11. Van Deerlin VM, Leverenz JB, Bekris LM, Bird TD, Yuan W, et al. (2008) TARDBP mutations in amyotrophic lateral sclerosis with TDP-43 neuropathology: a genetic and histopathological analysis. Lancet Neurol 7: 409–416.
12. Pesiridis GS, Lee VM, Trojanowski JQ (2009) Mutations in TDP-43 link glycine-rich domain functions to amyotrophic lateral sclerosis. Hum Mol Genet 18: R156–R162.
13. Benajiba L, Le Ber I, Camuzat A, Lacoste M, Thomas-Anterion C, et al. (2009) TARDBP mutations in motoneuron disease with frontotemporal lobar degeneration. Ann Neurol 65: 470–473.
14. Kovacs GG, Murrell JR, Horvath S, Haraszti L, Majtenyi K, et al. (2009) TARDBP variation associated with frontotemporal dementia, supranuclear gaze palsy, and chorea. Mov Disord 24: 1843–1847.
15. Kwiatkowski TJ Jr, Bosco DA, Leclerc AL, Tamrazian E, Vanderburg CR, et al. (2009) Mutations in the FUS/TLS gene on chromosome 16 cause familial amyotrophic lateral sclerosis. Science 323: 1205–1208.
16. Vance C, Rogelj B, Hortobágyi T, De Vos KJ, Nishimura AL, et al. (2009) Mutations in FUS, an RNA processing protein, cause familial amyotrophic lateral sclerosis type 6. Science 323: 1208–1211.
17. Hewitt C, Kirby J, Highley JR, Hartley JA, Hibberd R, et al. (2010) Novel FUS/TLS mutations and pathology in familial and sporadic amyotrophic lateral sclerosis. Arch Neurol 67: 455–461.
18. Broustal O, Camuzat A, Guillot-Noël L, Guy N, Millecamps S, et al. (2010) FUS mutations in frontotemporal lobar degeneration with amyotrophic lateral sclerosis. J Alzheimers Dis 22: 765–769.
19. Mackenzie IR, Rademakers R, Neumann M (2010) TDP-43 and FUS in amyotrophic lateral sclerosis and frontotemporal dementia. Lancet Neurol 9: 995–1007.
20. Munoz DG, Neumann M, Kusaka H, Yokota O, Ishihara K, et al. (2009) FUS pathology in basophilic inclusion body disease. Acta Neuropathol 118: 617–627.
21. Huang EJ, Zhang J, Geser F, Trojanowski JQ, Strober JB, et al. (2010) Extensive FUS-immunoreactive pathology in juvenile amyotrophic lateral sclerosis with basophilic inclusions. Brain Pathol 20: 1069–1076.
22. Urwin H, Josephs KA, Rohrer JD, Mackenzie IR, Neumann M, et al. (2010) FUS pathology defines the majority of tau- and TDP-43-negative frontotemporal lobar degeneration. Acta Neuropathol 120: 33–41.
23. Lagier-Tourenne C, Cleveland DW (2009) Rethinking ALS: the FUS about TDP-43. Cell 136: 1001–1004.
24. Doi H, Koyano S, Suzuki Y, Nukina N, Kuroiwa Y (2010) The RNA-binding protein FUS/TLS is a common aggregate-interacting protein in polyglutamine diseases. Neurosci Res 66: 131–133.
25. Woulfe J, Gray DA, Mackenzie IR (2010) FUS-immunoreactive intranuclear inclusions in neurodegenerative disease. Brain Pathol 20: 589–597
26. Crozat A, Aman P, Mandahl N, Ron D (1993) Fusion of CHOP to a novel RNA-binding protein in human myxoid liposarcoma. Nature 363: 640–644.
27. Zinszner H, Sok J, Immanuel D, Yin Y, Ron D (1997) TLS (FUS) binds RNA in vivo and engages in nucleo-cytoplasmic shuttling. J Cell Sci 110: 1741–1750.
28. Kasyapa CS, Kunapuli P, Cowell JK (2005) Mass spectroscopy identifies the splicing-associated proteins, PSF, hnRNP H3, hnRNP A2/B1, and TLS/FUS as interacting partners of the ZNF198 protein associated with rearrangement in myeloproliferative disease. Exp Cell Res 309: 78–85.
29. Andersson MK, Ståhlberg A, Arvidsson Y, Olofsson A, Semb H, et al. (2008) The multifunctional FUS, EWS and TAF15 proto-oncoproteins show cell type-specific expression patterns and involvement in cell spreading and stress response. BMC Cell Biol 9: 37–54.
30. Fujii R, Okabe S, Urushido T, Inoue K, Yoshimura A, et al. (2005) The RNA binding protein TLS is translocated to dendritic spines by mGluR5 activation and regulates spine morphology. Curr Biol 15: 587–593.
31. Lee BJ, Cansizoglu AE, Süel KE, Louis TH, Zhang Z, et al. (2006) Rules for nuclear localization sequence recognition by karyopherin beta 2. Cell 126: 543–558.
32. Dormann D, Rodde R, Edbauer D, Bentmann E, Fischer I, et al. (2010) ALS-associated fused in sarcoma (FUS) mutations disrupt Transportin-mediated nuclear import. EMBO J 29: 2841–2857.
33. Ito D, Seki M, Tsunoda Y, Uchiyama H, Suzuki N (2011) Nuclear transport impairment of amyotrophic lateral sclerosis-linked mutations in FUS/TLS. Ann Neurol 69: 152–162.
34. Kino Y, Washizu C, Aquilanti E, Okuno M, Kurosawa M, et al. (2011) Intracellular localization and splicing regulation of FUS/TLS are variably affected by amyotrophic lateral sclerosis-linked mutations. Nucleic Acids Res 39: 2781–2798.
35. Bosco DA, Lemay N, Ko HK, Zhou H, Burke C, et al. (2010) Mutant FUS proteins that cause amyotrophic lateral sclerosis incorporate into stress granules. Hum Mol Genet 19: 4160–4175.
36. Stolow DT, Haynes SR (1995) Cabeza, a *Drosophila* gene encoding a novel RNA binding protein, shares homology with EWS and TLS, two genes involved in human sarcoma formation. Nucleic Acids Res 23: 835–843.
37. Feiguin F, Godena VK, Romano G, D'Ambrogio A, Klima R, et al. (2009) Depletion of TDP-43 affects Drosophila motoneurons terminal synapsis and locomotive behavior. FEBS Lett 583: 1586–1592.
38. Lagier-Tourenne C, Polymenidou M, Cleveland DW (2010) TDP-43 and FUS/TLS: emerging roles in RNA processing and neurodegeneration. Hum Mol Genet 19: R46–R64.
39. DeJesus-Hernandez M, Kocerha J, Finch N, Crook R, Baker M, et al. (2010) De novo truncating FUS gene mutation as a cause of sporadic amyotrophic lateral sclerosis. Hum Mutat 31: E1377–E1389.
40. Sun Z, Diaz Z, Fang X, Hart MP, Chesi A, et al. (2011) Molecular determinants and genetic modifiers of aggregation and toxicity for the ALS disease protein FUS/TLS. PLoS Biol 9: e1000614.
41. Buratti E, Baralle FE (2009) The molecular links between TDP-43 dysfunction and neurodegeneration. Adv Genet 66: 1–34.
42. Wegorzewska I, Bell S, Cairns NJ, Miller TM, Baloh RH (2009) TDP-43 mutant transgenic mice develop features of ALS and frontotemporal lobar degeneration. Proc Natl Acad Sci U S A 106: 18809–18814.
43. Kabashi E, Lin L, Tradewell ML, Dion PA, Bercier V, et al. (2010) Gain and loss of function of ALS-related mutations of TARDBP (TDP-43) cause motor deficits in vivo. Hum Mol Genet 19: 671–683.
44. Li Y, Ray P, Rao EJ, Shi C, Guo W, et al. (2010) A *Drosophila* model for TDP-43 proteinopathy. Proc Natl Acad Sci U S A 107: 3169–3174.
45. Wils H, Kleinberger G, Janssens J, Pereson S, Joris G, et al. (2010) TDP-43 transgenic mice develop spastic paralysis and neuronal inclusions characteristic of ALS and frontotemporal lobar degeneration. Proc Natl Acad Sci U S A 107: 3858–3863.
46. Hanson KA, Kim SH, Wassarman DA, Tibbetts RS (2010) Ubiquilin modifies TDP-43 toxicity in a *Drosophila* model of amyotrophic lateral sclerosis (ALS). J Biol Chem 285: 11068–11072.
47. Miguel L, Frébourg T, Campion D, Lecourtois M (2011) Both cytoplasmic and nuclear accumulations of the protein are neurotoxic in *Drosophila* models of TDP-43 proteinopathies. Neurobiol Dis 41: 398–406.
48. Lanson NA Jr, Maltare A, King H, Smith R, Kim JH, et al. (2011) A *Drosophila* model of FUS-related neurodegeneration reveals genetic interaction between FUS and TDP-43. Hum Mol Genet 20: 2510–2523.
49. Igaz LM, Kwong LK, Lee EB, Chen-Plotkin A, Swanson E, et al. (2011) Dysregulation of the ALS-associated gene TDP-43 leads to neuronal death and degeneration in mice. J Clin Invest 121: 726–738.
50. Wang JW, Brent JR, Tomlinson A, Shneider NA, McCabe BD (2011) The ALS-associated proteins FUS and TDP-43 function together to affect Drosophila locomotion and life span. J Clin Invest 121: 4118–4126.
51. Hicks GG, Singh N, Nashabi A, Mai S, Bozek G, et al. (2000) Fus deficiency in mice results in defective B-lymphocyte development and activation, high levels of chromosomal instability and perinatal death. Nat Genet 24: 175–179.

52. Fujii R, Okabe S, Urushido T, Inoue K, Yoshimura A, et al. (2005) The RNA binding protein TLS is translocated to dendritic spines by mGluR5 activation and regulates spine morphology. Curr Biol 15: 587–593.
53. Kuroda M, Sok J, Webb L, Baechtold H, Urano F, et al. (2000) Male sterility and enhanced radiation sensitivity in TLS(-/-) mice. EMBO J 19: 453–462.
54. Stewart BA, Mohtashami M, Rivlin P, Deitcher DL, Trimble WS, et al. (2002) Dominant-negative NSF2 disrupts the structure and function of *Drosophila* neuromuscular synapses. J Neurobiol 51: 261–271.
55. Takahashi Y, Hirose F, Matsukage A, Yamaguchi M (1999) Identification of three conserved regions in the DREF transcription factors from *Drosophila melanogaster* and *Drosophila virilis*. Nucleic Acids Res 27: 510–516.
56. Kondo T, Inagaki S, Yasuda K, Kageyama Y (2006) Rapid construction of *Drosophila* RNAi transgenes using pRISE, a P-element-mediated transformation vector exploiting an in vitro recombination system. Genes Genet Syst 81: 129–134.
57. Spradling AC (1986) P-element-mediated transformation. In: Roberts DB, editor, *Drosophila*: a practical approach. Oxford: IRL Press.
58. Robertson HM, Preston CR, Phillis RW, Johnson-Schlitz DM, Benz WK, et al. (1988) A stable genomic source of P element transposase in *Drosophila melanogaster*. Genetics 118: 461–470.
59. Nagai R, Hashimoto R, Tanaka Y, Taguchi O, Sato M, et al. (2010) Syntrophin-2 is required for eye development in *Drosophila*. Exp Cell Res 316: 272–285.
60. Stewart BA, Atwood HL, Renger JJ, Wang J, Wu CF (1994) Improved stability of *Drosophila* larval neuromuscular preparations in haemolymph-like physiological solutions. J Comp Physiol A 175: 179–191.
61. Shcherbata HR, Yatsenko AS, Patterson L, Sood VD, Nudel U, et al. (2007) Dissecting muscle and neuronal disorders in a Drosophila model of muscular dystrophy. EMBO J 26: 481–493.
62. Prasad DD, Ouchida M, Lee L, Rao VN, Reddy ES (1994) TLS/FUS fusion domain of TLS/FUS-erg chimeric protein resulting from the t(16;21) chromosomal translocation in human myeloid leukemia functions as a transcriptional activation domain. Oncogene 9: 3717–3729.
63. Cushman M, Johnson BS, King OD, Gitler AD, Shorter J (2010) Prion-like disorders: blurring the divide between transmissibility and infectivity. J Cell Sci 123: 1191–1201.
64. Udan M, Baloh RH (2011) Implications of the prion-related Q/N domains in TDP-43 and FUS. Prion 5: 1–5.
65. Lerga A, Hallier M, Delva L, Orvain C, Gallais I, et al. (2001) Identification of an RNA binding specificity for the potential splicing factor TLS. J Biol Chem 276: 6807–6816.
66. Iko Y, Kodama TS, Kasai N, Oyama T, Morita EH, et al. (2004) Domain architectures and characterization of an RNA-binding protein, TLS. J Biol Chem 279: 44834–44840.

その他のFTLD — 異常蛋白の視点から

上山盛夫　藤掛伸宏　永井義隆

はじめに

前頭側頭葉変性症(FTLD：frontotemporal lobar degeneration)は前頭葉と側頭葉の神経が進行性に変性・脱落する神経変性疾患である．病理型としては，多くの神経細胞あるいはグリア細胞内に封入体が認められるFTLDと，封入体が認められないFTLD-ni(no inclusions)に大別され，封入体が認められるものは，蓄積する蛋白質によりFTLD-tau，FTLD-TDP，FTLD-FUS，およびFTLD-UPS(ubiquitin proteasome system)の4型に分類されている[1]．本稿ではFTLD-tau以外の封入体が認められるFTLD-Uについて異常蛋白質の視点から紹介する．また，近年FTLDの原因として同定された*C9orf72*遺伝子変異による異常蛋白質の蓄積についても最新の知見を紹介する．

うえやま もりお　(独)国立精神・神経医療研究センター神経研究所/疾病研究第四部
ふじかけ のぶひろ　同
ながい よしたか　同 室長

FTLD-TDP

タウ陰性でユビキチン陽性の封入体を伴ったFTLD-Uにおいて，封入体を構成する主要蛋白質は不明であったが，2006年にRNA結合蛋白質であるTAR DNA-binding protein of 43(TDP-43)が蓄積していることが明らかにされた[2,3]．FTLD-Uのうち TDP-43陽性封入体の病理所見を示すものはFTLD-TDPと分類され，FTLDの45%を占める[4]．さらに，筋萎縮性側索硬化症(ALS：amyotrophic lateral sclerosis)においてもTDP-43が蓄積していることが明らかにされたことから，FTLDとALS両疾患の病態には共通の分子基盤があると考えられるようになった．TDP-43はFTLD-TDP患者脳内において疾患特異的なリン酸化や断片化を受けており，特にC末断片の凝集・蓄積が観察される[5,6]．TDP-43のC末端には凝集性に富むプリオン様ドメインが存在し(図1)，断片化により凝集性が増すことから，このC末断片が患者脳における凝集・蓄積

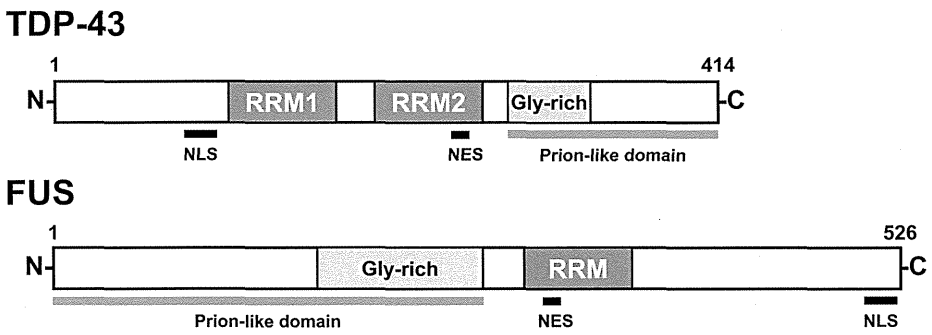

図1　TDP-43とFUSの蛋白質構造

TDP-43は414残基，FUSは526残基のアミノ酸からなり，その分子内にはRNA結合に関わるRNA認識モチーフ(RRM：RNA recognition motif)，蛋白質-蛋白質相互作用に関わるグリシンリッチ領域(Gly-rich)を含むプリオン様ドメイン(Prion-like domain)，核移行シグナル(NLS：nuclear localization signal)，および核外移行シグナル(NES：nuclear export signal)が存在する．

0289-0585/15/¥500/論文/JCOPY

に関与すると予測される．異常なTDP-43の凝集・蓄積メカニズムおよび細胞間伝播は未解明であったが，2013年にNonakaらは，患者脳由来の不溶性TDP-43を培養細胞内に導入すると，本来は可溶性であった細胞内のTDP-43が凝集体を形成することを示し，異常TDP-43の凝集性が正常TDP-43に伝播すること，さらにこのTDP-43の凝集性は細胞間でも伝播することを明らかにした．これらの結果から，患者脳の不溶性TDP-43はプリオン様の特性を保持していると結論付けている[7]．培養細胞を用いた*in vitro*の実験ではあるが，TDP-43の凝集・蓄積モデルを樹立し，細胞間伝播までを示した上記の研究は興味深いものであり，今後，動物モデルや患者病理の解析からTDP-43のプリオン様の性質獲得と病態の進行との関連性の解明が期待される．

FTLD-FUS

2008年に家族性ALS(ALS6)の原因としてFUS変異が同定され，ALS6患者の病理学的解析からFUSが神経細胞質内の封入体の構成成分であることが明らかにされた．続いて，TDP-43陰性封入体を伴ったaFTLD-U(atypical FTLD-U)，NIFID(neuronal intermediate filament inclusion disease)，とBIBD(basophilic inclusion body disease)において，神経細胞およびグリア細胞の細胞質にFUS陽性の封入体が認められることが明らかになり[8~10]，これらはまとめてFTLD-FUSと分類された．RNA結合蛋白質であるFUSはTDP-43と同様に，分子内に凝集性に富むプリオン様ドメインを持っていることから(図1)，FTLD-TDPで認められている異常蛋白質の伝播がFTLD-FUSでも生じる可能性が示唆される．しかし，FUSが凝集・蓄積するメカニズムは未解明であり，今後の研究が必要である．

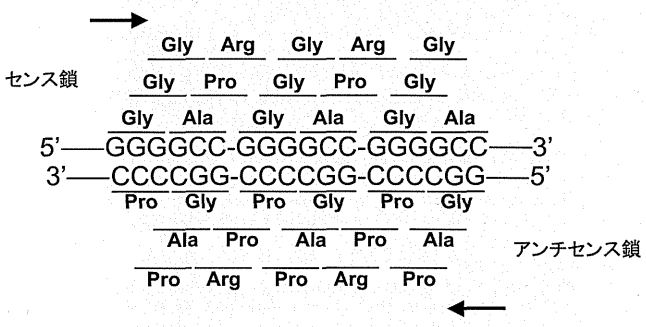

図2 *C9orf72*遺伝子GGGGCC異常伸長リピート由来のジペプチドリピート蛋白質

C9-FTLD/ALS患者において*C9orf72*遺伝子非翻訳領域の6塩基(GGGGCC)異常伸長リピート配列はセンス鎖およびアンチセンス鎖の両方向に転写される．さらに，ATGに依存しない翻訳(RANT：repeat-associated non-ATG translation)により5種類のジペプチドリピート(DPR：dipeptide repeat)蛋白質が産生される．Gly：グリシン，Arg：アルギニン，Pro：プロリン，Ala：アラニン

FTLD-UPS

FTLD-Uのうち TDP-43陰性およびFUS陰性で，未だその主要構成成分の不明な封入体を伴うものはFTLD-UPSと分類されている．そのうちの一部において*CHMP2B*(charged multivesicular body protein 2B)の遺伝子変異が明らかにされた[11]．CHMP2Bはエンドソーム輸送選別複合体を構成する分子で，リソソームにおけるユビキチン化蛋白質の分解に関与することが知られており，CHMP2Bの機能不全によりユビキチン化蛋白質が細胞質内に残留し，封入体を形成していると考えられる．

最近の話題 — C9-FTLD/ALS

2006年にALS-FTD家系の連鎖解析から第9番染色体に原因遺伝子座があると報告された．その遺伝子変異は長らく不明であったが，2011年にこの家族性ALS-FTDの原因遺伝子変異として染色体9p21領域に存在する*C9orf72*遺伝子の非翻訳領域に6塩基(GGGGCC)リピート配列の異常伸長が発見された[12,13]．この*C9orf72*遺伝子変異はヨーロッパおよび北米の家族性と孤発性FTLD/ALSの最も高頻度な発症原因であり，本邦でも紀伊半島のFTLD/ALS家系を中心に報告されている．*C9orf72*遺伝子変異によるFTLD/ALS(C9-FTLD/ALS)患者ではTDP-43陽性を示す封入体が脳の広範囲でみられ，FTLD-TDPに分類されているが，小脳，海馬，および前頭側頭新皮質ではTDP-43陰性の封入体が認められる[14]．C9-FTLD/ALSと同様な遺伝子非翻訳領域にあるリピート配列の異常伸長に起因するSCA8，DM1，およびFXTASなどの一群の疾患では，転写された異常伸長リピートRNAを鋳型として開始コドンATGに依存しない翻訳(RANT：repeat-associated non-ATG translation)により，